

11-10-2020

Opto-Fluidic Manipulation of Microparticles and Related Applications

Hao Wang
University of South Florida

Follow this and additional works at: <https://digitalcommons.usf.edu/etd>



Part of the [Biomedical Engineering and Bioengineering Commons](#)

Scholar Commons Citation

Wang, Hao, "Opto-Fluidic Manipulation of Microparticles and Related Applications" (2020). *USF Tampa Graduate Theses and Dissertations*.
<https://digitalcommons.usf.edu/etd/8601>

This Dissertation is brought to you for free and open access by the USF Graduate Theses and Dissertations at Digital Commons @ University of South Florida. It has been accepted for inclusion in USF Tampa Graduate Theses and Dissertations by an authorized administrator of Digital Commons @ University of South Florida. For more information, please contact digitalcommons@usf.edu.

Opto-Fluidic Manipulation of Microparticles and Related Applications

by

Hao Wang

A dissertation submitted in partial fulfillment
of the requirements for the degree of
Doctor of Philosophy in Biomedical Engineering
Department of Medical Engineering
College of Engineering
University of South Florida

Major Professor: Anna Pyayt, Ph.D.
Robert Frisina, Ph.D.
Steven Saddow, Ph.D.
Sandy Westerheide, Ph.D.
Piyush Koria, Ph.D.

Date of Approval:
October 30, 2020

Key words: Thermal-plasmonic, Convection, Microfluid, Aggregation, Isolation

Copyright © 2020, Hao Wang

Dedication

This dissertation is dedicated to the people who have supported me throughout my education. Great appreciation to my academic adviser Dr. Anna Pyayt who kept me on track. Special thanks to my wife Qun, who supports me for years since the beginning of our marriage.

Thanks for making me see this adventure though to the end.

Acknowledgments

On the very outset of this dissertation, I would like to express my deepest appreciation towards all the people who have helped me in this endeavor. Without their warmly guidance, help, cooperation, and encouragement, I would not be able to make headway in the project.

I am extremely thankful and pay my earnest gratitude to my advisor Dr. Anna Pyayt. Every step forward in my research cannot be made without your support.

I am also ineffably indebted to every single professor in my committee: Dr. Robert Frisina, Dr. Stephen Sadow, Dr. Sandy Westerheide and Dr Piyush Koria. Your encouragement and instruction will guide me complete the journey, as the dawn light on horizon.

I extend my gratitude to Dr. Prahathees Eswara for your support and offering me chance of cooperation.

Finally, gratitude goes to all my colleagues and friends who help me directly or indirectly to complete my research.

Any omission in this brief acknowledgement does not mean lack of gratitude.

Table of Contents

List of Tables.....	iii
List of Figures.....	iv
Abstract.....	vii
Chapter 1: Mechanism of Opto-Fluidics and Structure Optimization of Substrate.....	1
1.1 Optimization of Structure.....	5
1.2 Conclusion.....	9
Chapter 2: Simulations of Opto-Fluidics and Experimental Verification.....	10
2.1 Simulation Settings.....	12
2.1.1 Theoretical Simulations, Assumptions and Simplifications.....	13
2.1.2 Simulations of Fluid Mechanics.....	14
2.1.3 Simulations of Heat Transfer.....	14
2.2 Results of Simulations and Experiments.....	16
2.2.1 Horizontal Substrate without Additional Flow in Channel.....	16
2.2.2 Microfluidic Channel with an External Flow.....	17
2.2.3 Tilted Microfluidic Channel without an External Flow.....	20
2.3 Conclusion.....	21
Chapter 3: Microparticles Manipulation by Using Opto-Fluidic Chip.....	22
3.1 Methods and Experiment Results.....	24
3.2 Conclusion and Discussion.....	35
Chapter 4: Biocompatibility Test of Opto-Fluidic Chip.....	36
4.1 Methods and Experiment Results.....	36
4.2 Conclusion.....	42
Chapter 5: Bacteria Separation Using Opto-Fluidic System.....	43
5.1 Methods.....	46
5.2 Experiment Results.....	49
5.2.1 Concentration of Bacteria.....	49
5.2.2 Isolation of Bacteria.....	53
5.2.3 Rapid Antibiotic Screening.....	55
5.3 Conclusion.....	56
Chapter 6: Opto-Fluidics Induced Antibody Immobilization-Based Rapid Detection.....	58
6.1 Methods and Experiment Results.....	60

Chapter 7: Accomplishments and Involvements in Other Projects.....	69
7.1 Subcellular and in-vivo Nano-Endoscopy.....	69
7.2 Plasmono-Magnetic Material for Precise Photothermal Heating.....	70
7.3 Modular Microfluidic Filters Based on Transparent Membranes.....	72
7.4 Measurement of Thickness of Highly Inhomogeneous Crude Oil Slicks.....	73
References.....	74
Appendix 1: Copyright Permissions.....	79

List of Tables

Table 6.1 Table contains 6 values of green color intensity which extracted from fluorescent microscope images.....	62
Table 6.2 Table contains 2*8 fluorescent microscope images.....	64
Table 6.3 Table contains 3*4 fluorescent microscope images.....	67

List of Figures

Figure 1.1 Photos of thermal-plasmonic substrate.....	5
Figure 1.2 The substrate optimization.....	7
Figure 1.3 3-D sketch showing the scene of heating up one droplet on substrate.....	8
Figure 2.1 2-D schematic showing the experimental set-up.....	13
Figure 2.2 2-D cross-section of the simulated temperature distribution and the streamline plot of a fluid sample in a cylindrical well.....	16
Figure 2.3 Images show particles manipulation in the cylindrical well.....	17
Figure 2.4 2-D cross-sectional temperature and velocity streamline plots for fluid flowing through the channel on the XZ and YZ planes (along and across the flow)	18
Figure 2.5 Images show particles manipulation in the channel with external flow.....	18
Figure 2.6 Change in the microfluidic flow pattern depending on the laminar flow introduced at the channel input.....	19
Figure 2.7 2-D cross-sectional temperature and velocity streamline plots of the channel tilted at 20° relative to the horizontal level.....	20
Figure 2.8 A 10X magnification microscopic image showing the microparticles aggregation on an inclined substrate.....	21
Figure 3.1 Pictures present the complete experimental set-up.....	27
Figure 3.2 2-D sketch of the experimental set-up.....	28
Figure 3.3 2-D sketch of Opto-Fluidic chip from the top view.....	29
Figure 3.4 Two sets of images show 5-micron and 10-micron particles manipulations.....	30
Figure 3.5 Images show the 20-micron particles manipulation.....	31

Figure 3.6 Images shows the separation of two types particles (5 micron and 20 micron) from a mixed particles aggregation via using the system.....	32
Figure 3.7 Images shows the capturing particles by using needle from flowing sample.....	34
Figure 4.1 Image shows the Opto-Fluidic chip for cell viability tests.....	38
Figure 4.2 Images show the normal cellular morphology of fibroblast cells in bright-field and fluorescence field.....	39
Figure 4.3 Demonstration of fibroblast cell viability after opto-fluidic manipulation.....	40
Figure 4.4 Images demonstrate that the majority cells in the bacteria aggregation are alive.....	41
Figure 5.1 Experimental setup and bacteria used for manipulation.....	48
Figure 5.2 Two sets of images demonstrate that both high (left set) and low (right set) concentrations of bacteria can be aggregated after 2 minutes of optofluidic manipulation.....	51
Figure 5.3 Optofluidic concertation of <i>E. coli</i>	52
Figure 5.4 Schematics of an experimental setup with a microfluidic channel for capturing of concentrated bacteria for further analysis followed by experimental results with DAPI-stained <i>B. subtilis</i>	54
Figure 5.5 Magnified view of the initial concentrated cluster of bacteria and one obtained after re-concentration.....	55
Figure 5.6 Fluorescence microscopy was used to determine the susceptibility of wild type (WT) and ampicillin-resistant (ampR) <i>E. coli</i> cells as well as WT and ampR <i>S. aureus</i> cells to the treatment of ampicillin.....	56
Figure 6.1 Images show fluorescence on gold surface of three samples.....	61
Figure 6.2 Images show fluorescence on gold surface of three different samples.....	61
Figure 6.3 2-D sketch shows original molecule layer structure on plasmonic substrate.....	63
Figure 6.4 2-D sketch shows upgraded molecule layer structure on substrate.....	63
Figure 6.5 Image shows the Opto-Fluidic chip which is used in experiments.....	64
Figure 6.6 Line chart demonstrates Opto-Fluidics in sample can speed up fluorescent antibody attachment.....	66

Figure 6.7 Line chart reveals the optimal settings of Opto-Fluidic treatment for the best outcome.....	68
Figure 7.1 In vitro spectrum collection using nanoendoscope.....	70
Figure 7.2 The necrocytosis of fibroblast cells induced by local heat.....	71
Figure 7.3 Human lung fibroblast cells captured and then grown for 3 days on the surface of microfilter membrane.....	72
Figure 7.4 Measurement of the thickness of a slick generated on artificial seawater.....	73

Abstract

Contemporary biomedical technologies introduce many new instruments that are important for diagnosis and treatment of the patients. Instrument that can do rapid detection of bacterial infections, and further direct medical practitioner to prescribe optimal antibiotics is highly desirable. But unfortunately, this instrument is not available yet. Ideally, this instrument has to be portable to be used at point-of-care. This means it has to be small and inexpensive, but still highly accurate. Another critical requirement for the instrument is that the test results have to be available promptly. Because in case of such complications of bacterial infections as sepsis, each additional hour needed for the test decreases patient's chance of survival. Traditional treatment of bacterial infections is relied on empirical prescription of antibiotics. This kind of treatment is very imprecise and may incur side effects in long term. Meanwhile, optimal prescription of antibiotics for treating bacterial infection relies on the body fluids tests of patient. Whereas the test often includes bacteria culture followed by antibiotic susceptibility testing. These steps are very time-consuming and as a consequence, which may cause a negative impact on patient's chance of survival. The goal of this project is to address the fundamental challenges of optimal antibiotic prescription and develop new instrument for rapid concentration and analysis of bacteria.

This dissertation introduces an innovative approach to bacterial analysis based on a new Opto-Fluidic Manipulation (OFM) technology that we proposed and published in several reputable journals. OFM can be integrated with microfluidics for careful and gentle manipulation of micro and nano-scale objects in miniature fluid samples. We designed and optimized special bi-layer

metallic substrates that can efficiently absorb laser light, locally heat fluids for couple of degrees and generate microscopic currents. These micro-currents can be used to concentrate and project particles, sort them based on their size, capture bacteria, and many other interesting applications. We demonstrated that OFM does not damage live cells, bacteria, and it can be used to carefully isolate desired type of the bacterial cells from fluid samples for further analysis. In addition to that, we showed that isolated live bacteria can be used for rapid antibiotic susceptibility testing. This way we can potentially isolate bacteria from a biological sample and identify the optimal antibiotic under one hour, in comparison with the traditional approaches that can often take from 24 to 72 hours.

There are seven chapters in this dissertation. Briefly, chapter one and two explain the mechanism of OFM and optimization process of the integrated chip fabrication. Chapters three, four and five present a system derives from a combination of Opto-Fluidic chip and auxiliary components and various tests of the system with different types of particles. Chapter six demonstrates our latest results on micro-mixing application of OFM that can be used for accelerated antigen-antibody-based sensing. Finally, there are several other projects that I have participated in during Ph.D. study. I briefly discuss my contribution to each project focusing on development of different biomedical devices. Future development of these biomedical instruments might enable many important applications for better, more affordable, and precise healthcare.

¹Chapter 1: Mechanism of Opto-Fluidics and Structure Optimization of Substrate

The Opto-Fluidics has an exclusive definition in this research. However, the word “Opto-Fluidics” can express different meanings in different research. In fact, Opto-Fluidics is a relatively new field which focus on manipulating fluids with light, includes a variety of applications. For example, it could be used to passively sort material base on its chirality via using chiral light in a fluidic environment [1]. Another interesting application is fabrication of complex 3D-shaped polymer in fluid using UV light [2]. Biomedical related applications include integration of absorption spectroscopy to determine the level of hemoglobin in plasma into a miniaturized microfluidic sensor with built-in filtration of blood cells [3]. Similarly, an optical fiber-based spectroscopic system can be used for identification of drug concentration in complex real-world fluids [4]. Alternatively, Opto-Fluidics can be used to manipulate individual droplets inside of microfluidic channels. For instance, there was demonstrated an optofluidic droplet router that can route and steer microdroplets using optically induced forces [5]. Another on-chip droplet manipulation device can be used to count droplets at ultrahigh rate based on their fluorescent signals [6]. Additionally, the optofluidic lenses is a rapid growing area of adaptive optics [7]. Optofluidic plasmonic microlenses can be used for label-free sorting of exosomes [8]. Microfluidics based plasmonic microarrays on chip can be incorporated into biosensing devices

¹Partial contents of this chapter were published in Micromachines...Reference [20](Winskas, John T., Wang, Hao., et al. "Different Regimes of Opto-fluidics for Biological Manipulation." Micromachines 10.12 (2019): 802.). Permission is included in Appendix: Copyright Permissions

[9] and a smartphone based optofluidic platform can be used to detect biomarkers in blood [10]. Other types of Opto-Fluidics can be based on thermo-plasmonics. Both the heat generation and fluid convection were induced by plasmonic nanostructures and could be applied for microscale mass transport [11]. Different plasmonic structures including metal nanoparticles can be used to generate local heat in fluids using lasers [12]. As a result, variety of micro-flow patterns can be enabled [13-19,20-21]. Early-on, simulations of the convection currents which induced by photo-heating of a single gold disk predicted very low fluid velocities [13]. However, the experimental studies showed much higher velocities [13–15]. Later, it was demonstrated that different types of plasmonic patterns arrays can greatly influence flow parameters [14]. In addition to that, further optimization was required for choice of an optimal wavelength of laser light controlling the current generation [13, 16–19].

In this research, the Opto-Fluidics we created refer to convective currents that induced by local heat on delicately designed thermal-plasmonic structure. This type of Opto-Fluidics can be generated on a chip and can manipulate tiny objects in fluid samples that contained in chip. As a matter of fact, the testing chip we invented is the core component of device that do rapid concentration and isolation of bacteria. If we look into the basic structure of chip, we can divide the chip into two pieces, one is a special microscope slide and another one is a PDMS made mold with inner structure. On one side of the microscope slide, there is delicately designed metallic structure. This metallic structure we built on microscope slide is called thermal-plasmonic structure. The microscope slide which possesses plasmonic structure can be regarded as plasmonic substrate. The transparent glass layer serves as framework in substrate. It is the plasmonic structure that works on the generation of Opto-Fluidics. When use the chip in experiments, the plasmonic substrate can generate Opto-Fluidics by taking laser radiation and the existence of Opto-Fluidics

is around the location of laser spot inside liquid. Meanwhile, the PDMS made mold contributes nothing for the generation of Opto-Fluidics. It is made to adhere on plasmonic substrate for the purpose of containing samples and facilitating particle isolation and collection. This chapter will elaborate the entire process of optimization of plasmonic structure for more effectively generating Opto-Fluidics in detail.

As mentioned earlier, the generation of Opto-Fluidics requires two basic elements: plasmonic substrate and laser. The plasmonic substrate can induce the thermo-plasmonic effect on its surface, by taking laser beam striking. This thermo-plasmonic effect as the dominating factor drives the transformation of energy from optical energy to thermal energy. This energy transformation takes place at exactly where the laser beam strikes on substrate. The local heat on substrate can lead to inner heat conduction of metallic structure. But more importantly, the heat will be conducted to liquid which is above substrate. Consequently, the locally heated liquid will induce heat convection. This is the second step of energy transformation, that indicates thermal energy converts to kinetic energy of fluid. This serial of energy transformation ultimately leads to the generation of convective flows around the heat spot. In this study, the entire collection of convective flows which are originated from laser radiation can clearly depict the term “Opto-Fluidics”. It is very obvious that the strength and location of Opto-Fluidics can be determined by laser beam. Furthermore, use the Opto-Fluidics to manipulate the group movement of micro objects in liquid is called OFM technology.

After we understand the mechanism of Opto-Fluidics, further research on the device is necessary for getting a more effective generation of Opto-Fluidics. Laser as one basic element and can influence the efficiency of generating Opto-Fluidics. Theoretically, there is not just one type of laser beam with stable power density and micron-scale diameter can be utilized for generating

Opto-Fluidics. However, we exclusively choose the laser beam which has a wavelength of 532 nm for doing all experiments that are mentioned in this dissertation. Meanwhile, we use the single mode optical fiber to guide laser beam, let the laser beam strikes on plasmonic substrate and forms a laser spot with diameter of couple hundreds of microns. The fixed settings on laser beam is critical for finding out the optimal plasmonic structure. That is because optimal plasmonic structure for a different wavelength of laser will be different.

Another element for generating Opto-Fluidics is the plasmonic substrate. The substrate consists of one microscope slide as framework and a metallic bi-layer structure built on one side of slide. The characters of metallic bi-layer structure can determine the efficiency of energy transformation, heat diffusion, and eventually affect the effective generation of Opto-Fluidics. The metallic structure consists of a uniform layer of chromium which coated on one side of slide and another uniform layer of gold which added on chromium layer. The sputtering system at USF NREC (Nanotechnology Research & Education Center) is utilized to deposit the thin metal layers on slide. When laser beam hits the substrate from the non-coated side, it will penetrate though glass and get absorbed by the layer of chromium. Meanwhile, a portion of the energy from laser can be converted into heat. Heat will be conducted to gold layer and to liquid sample. Eventually, local heat in liquid leads to the generation of Opto-Fluidics. As mentioned earlier, we utilize laser with a fixed wavelength in experiments, aim to identify an optimal plasmonic(metallic) structure which possesses the best compound optical absorption and total thermal conductivity, that allowing for the most effective generation of Opto-Fluidics.

1.1 Optimization of Structure

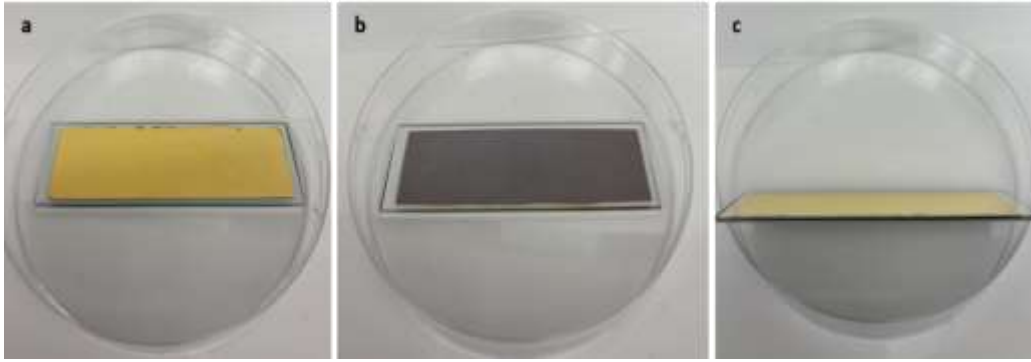


Figure 1.1 Photos of thermal-plasmonic substrate. Picture a, b and c show the appearance of substrate from different perspectives. The top view (a), bottom view (b) and side view (c).

Unlike other studies on plasmonic structure, which apply different 2D patterned shapes or nanoparticles, we choose to use the continuous bi-layer structure (showed in Figure 1.1). This choice was made based on the demonstration of COMSOL simulations. Simulations revealed a correlation between the thermal conductivity of the substrate and the efficiency of the convective current generation and its velocity. Figure 1.2a demonstrates that by heating three differently structured substrates (continuous gold layer, continuous chromium layer, and gold islands) to the same temperature, a noticeable difference in the fluid velocity presents. A reasonable explanation is that gold has much higher thermal conductivity than chromium, resulting in a much powerful convective flows induced in the liquid. The gold islands structure (made in gold) is observed to be the least efficient due to its discontinuity of heat conduction, compare with continuous structure. Consequently, the optimal structure should be in form of continuous layer and possessing high thermal conductivity. Thereupon, this continuous gold layer structure which conforms to both factors shall be the optimal option.

After determining the requirements for the thermal conductivity of the substrate, the next step is to take both optical and biocompatibility properties into consideration. The metallic bi-layer structure was chosen because there is no metallic single layer could simultaneously satisfy all

requirements: high thermal conductivity, good biocompatibility, and high optical absorption for the chosen wavelengths (532 nm). Chromium is chosen for making one layer because of its high absorption for chosen wavelength. The gold layer above chromium layer can function as a protection layer and reflector. On one hand, gold is generally biocompatible to cells and tissues. On the other hand, gold layer can block laser that penetrates through chromium layer and protect the sample from radiation damage caused by laser. Furthermore, gold layer also functions as reflector that can reflect laser back to chromium layer for re-absorption. Other kinds of metals like silver and copper have better thermal conductivity and can also reflect laser. But neither silver nor copper is as biocompatible as gold. This drawback limits the usage of silver and copper in our design since the substrate will have direct contact with biological samples in tests.

The individual metal layer thickness is studied to optimize overall performance after the material and bi-layer structure is determined. We conducted finite difference time domain (OptiFDTD) simulations to determine the thickness of metal layer for an optimal optical absorption. The gold layer thickness was chosen to be 200 nm for optimal reflection. Meanwhile, the thickness of the chromium layer was varied between 0 and 100 nm in the simulations (Figure 1.2b). Chromium and gold were both modeled as Lorentz–Drude dispersive materials. To match experimental setting, the light with wavelength of 532 nm is applied in simulation. Several important settings in simulation are subject to the experimental conditions, such as the laser beams are linearly polarized, have a Gaussian profile, are emitting continuously, are perpendicularly strikes to the substrate.

The absorption by bi-metallic structure with respect to the chromium thickness is plotted in Figure 1.2b. Since gold is highly reflective, adding a layer of 200 nm gold on top of chromium effectively doubles the propagation length of the light in chromium layer. The absorption of the bi-layer reaches the highest at 5 nm thickness of chromium for 532 nm light. Not surprisingly, the

optimized absorption by the layered structure is higher than absorption by a single layer of chromium. This is the result of multiple reflections in the low-quality factor plasmonic resonator consisting of a metallic bi-layer on a glass slide.

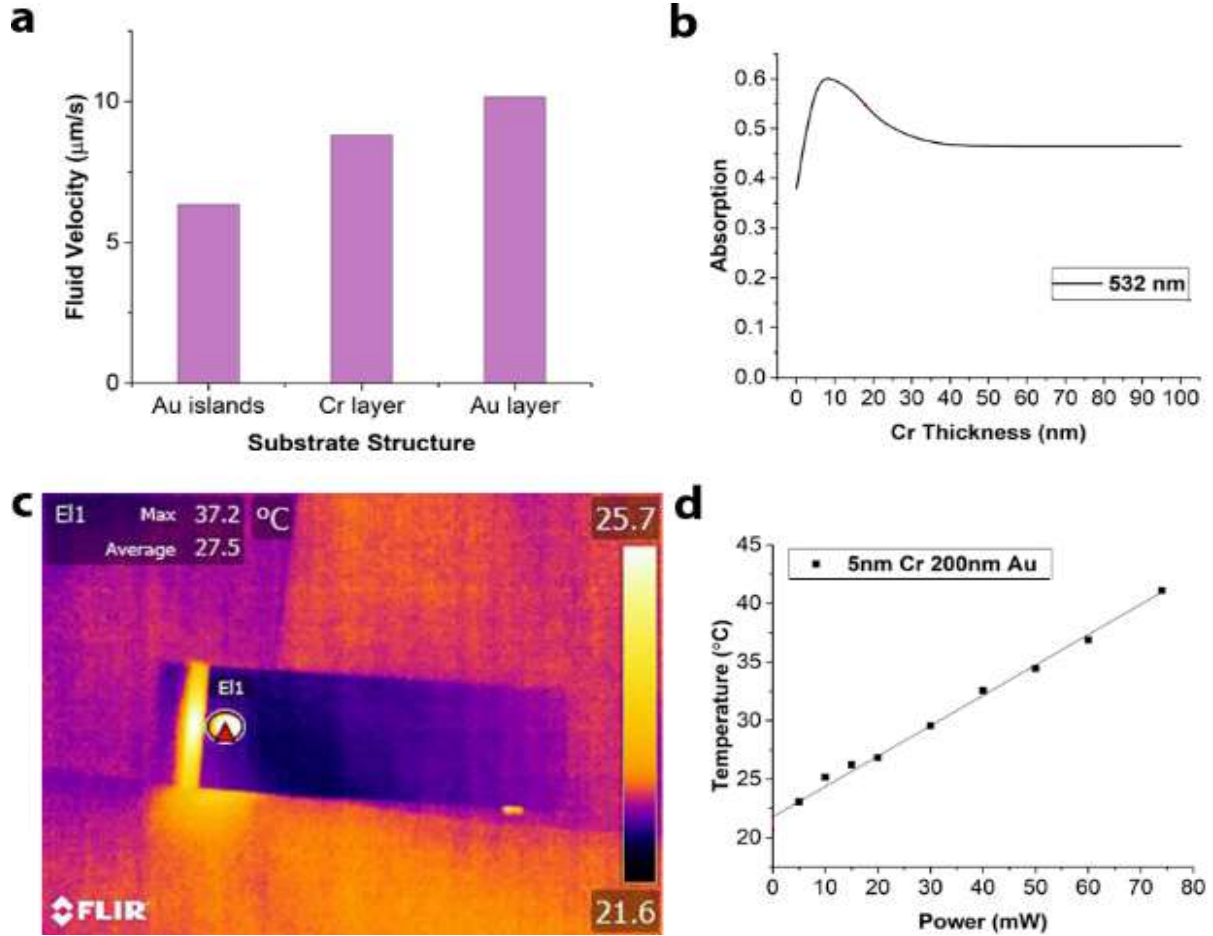


Figure 1.2 The substrate optimization. (a) COMSOL simulations were conducted to evaluate the most efficient substrate structure. (b) Finite difference time domain (FDTD) simulation results for substrate absorption optimization for 532 wavelength varying chromium thickness from 0 to 100 nm while holding gold thickness constant at 200 nm. (c) FLIR IR camera imaging was used to measure the maximum temperature in a 1 μL drop of fluid. (d) Experimentally measured temperature increase while testing the substrate with 532 nm light with power ranging from 0 to 80 mW.

Based on the results of the simulations, the optimized plasmonic structure for 532 nm lasers is determined (5nm-Cr / 200nm-Au). Then, this bi-layer structure is deposited on side of glass slide by sputtering. Subsequently, the performance of the substrate is evaluated in experiment. A FLIR

thermal camera is used to measure temperatures. From the images taken by FLIR thermal camera (Figure 1.2c), we can tell the substrate can efficiently absorb laser and heat a 1 μ l drop of water which was placed on top of the substrate. The maximum equilibrium temperature of water drop can be reached within 1–2 minutes under laser exposure. As the power of the laser gradually increases from 0 to 80 mW, the temperature of the water droplet increased linearly from 23 $^{\circ}$ C to 40 $^{\circ}$ C (Figure 1.2d). Here the 23 $^{\circ}$ C is the ambient temperature. This result, when combines with the linear relationship between the temperature and the fluid velocity vectors observed in COMSOL simulations, allow us to infer a linear relationship between the fluid velocity in the generated convective currents and the laser power. Additionally, this linear relationship leads to the conclusion that an increase of 4 mW of the laser power can result in a water droplet (1 μ l) temperature increase of 1 $^{\circ}$ C correspondingly.

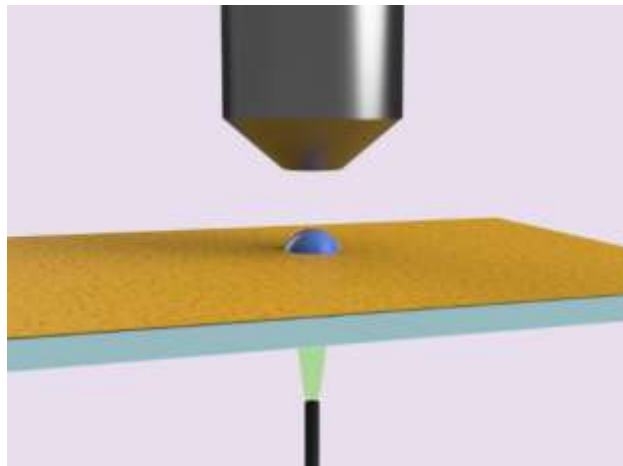


Figure 1.3 3-D sketch showing the scene of heating up one droplet on substrate. From top to bottom are microscope lens, droplet on top of thermo-plasmonic substrate, 532 nm laser beam and optical fiber.

Figure 1.3 is a 3D sketch that clearly depicts the simplified set-up for temperature measurement of droplet on substrate. While the laser light is coupled into an optical fiber that has been cleaved on one end. The fiber is inserted into a fiber holder and attached to a micromanipulator allowing XYZ fiber movement. After aligning the cleaved fiber tip underneath the microscope objective,

we place the plasmonic substrate horizontally between the fiber and the objective. Because the microscope lens and fiber are vertically aligned, we can use the light from upright microscopic to pinpoint the location of laser spot at the top surface of substrate. Then, we place a droplet of water on top of the gold surface where at the position of laser spot. Next, the laser is turned on and it strikes the substrate from bottom. Finally, the tiny droplet of water is heated, and the temperature changes of droplet are recorded by the thermal camera in real time.

1.2 Conclusion

In this chapter, the structure of plasmonic substrate is optimized under a particular wavelength of light (532 nm), for the most effective generation of Opto-Fluidics. Meanwhile, simulations and experiment results demonstrate that the fluid velocity of the convective vortices has linear relationship with the temperature of the heat source, which is also linearly proportional to the laser power. As the foundation of following research, we use this optimized plasmonic substrate to make Opto-Fluidic chip. This chip allows using OFM technology to process liquid samples. Additionally, the in-depth understanding of plasmonic substrate enable us to have a better control over Opto-Fluidics and to have a better control over the manipulation on desired microparticles from sample.

²Chapter 2: Simulations of Opto-Fluidics and Experimental Verification

The purpose of generating Opto-Fluidics on plasmonic substrate is conducting microparticle manipulation. Similarly, to the best of our knowledge, the most common and reproducible methods of microscale manipulation have included mechanical and magnetic micro-manipulators [22,23] and various types of optical tweezers [24] including: holographic [25], plasmonic [26], antenna-based [27], and photonic crystal-based tweezers [28]. While these methods work well on smaller particles and nano- scale objects [29,30], they are limited in their application to biological specimens. They might induce severe heating of biological material [31] and phototoxicity [32]. More recently, magnetic levitation of cells has allowed for 3D manipulation of biological specimen and sensing capabilities that are unachievable using traditional 2D manipulation of cells, however it requires the use of special magnetic fluids that are not compatible with many biological applications [23]. An alternative approach to cell manipulation is to use optofluidic tweezers (OFT) in capillaries [27] or thermally induced current generation by absorption in amorphous silicon [33] using a light source focused through a microscope objective. These approaches are fundamentally different from the traditional optical and optoelectronic tweezers, and magnetic levitation, as they can attain much stronger forces [34,35].

²The content of this chapter is in preparation by the Applied Optics. Permission is included in Appendix: Copyright Permissions

Most recently, a thermo-plasmonic approach to OFT has appeared as the next generation of micro-manipulation techniques. In plasmon-assisted microfluidics, plasmonic heating is used to generate convective flow patterns [13–19]. Initially, simulations include the modeling of convection currents induced by photo-heating a single gold disk [13], which predict very low fluid velocities in nm/s range. Later, it is demonstrated that localized heating of plasmonic structures can produce theoretically predicted toroid-shaped convection patterns [13–15]. Consequently, arrays of different plasmonic patterns are demonstrated [14], and this help to somewhat increase the velocity. The currents can be generated by heating with different wavelengths of light in the near IR spectrum shining on a variety of plasmonic structures and rough metal films [13,16–19]. However, only small particles can be manipulated without causing significant heating. The main reason for that is a prior focus on optical properties of the whole system while ignoring its thermal properties. Later, it is demonstrated that the thermal conductivity of the substrate plays an important role in the efficiency of the current generation. By adding continuous indium tin oxide (ITO) film to the substrate, the fluid velocity increases, and small particles are able to move with the speeds of up to 2 $\mu\text{m/s}$ [36]. In addition to that, much faster flow can be demonstrated using thermo-plasmonic heating with the generation of a water vapor microbubble, but this requires a pretty high temperature of operation [37,38]. However, in all these approaches to OFT the manipulated objects are exposed to significant amount of light radiation that could potentially damage cells or interfere with fluorescent imaging. Also, they are done using light coupled through a microscope objective, which makes the whole setup inflexible in terms of independent observation and manipulation. Finally, they support manipulation of small particles on flat surfaces, while we, for the first time, propose 3D manipulation and movement of larger objects and live cells, truly pushing the limit of micromanipulation while using a very low controlling laser power.

In the first chapter, the mechanism of Opto-Fluidics has been elaborated in detail. The Opto-Fluidics represent the entire collection of convective flows which is generated on top of plasmonic substrate. To better identify the patterns of convective flows and to get a better control over the Opto-Fluidics for particle manipulations, we first use simulation software to virtually generate Opto-Fluidics. Then by study the simulation models of Opto-Fluidics, we can visualize the patterns of convective flows in real Opto-Fluidics and explore the optimal condition of Opto-Fluidics for particles manipulation.

In this chapter, we study three different regimes of Opto-Fluidic manipulation in three configurations. The first configuration is a circular well without any external flow. The second configuration is a microfluidic channel with additional external flow. Finally, the third configuration is a tilted microfluidic channel without external flow. In order to explain all intriguing phenomena that we observe in the experiments, we use COMSOL Multiphysics simulations that help us to visualize temperature distributions and the shape of the convective flow. After that we conduct the experiments for each simulated configuration and use micro-particles for tracing the currents. The simulations are conducted using the Thermo-Hydro-Mechanical module from the COMSOL Multiphysics Modeling Software. All the parameters that are required for the simulation (e.g. temperature of the substrate, bi-metal composition, etc.) were taken from the measurements conducted in chapter one.

2.1 Simulation Settings

Figure 2.1 briefly depicts experimental set-up. As the core component, the chip lies in between microscope lens and optical fiber. The chip consists of a PDMS made container and plasmonic substrate. The PDMS container comes in various forms can adhere to substrate. The container in shape of hollow cylinder or well can hold static liquid sample. Meanwhile, container with channel

structure allows sample to flow in space of channel. While the microscope lens enables us to observe fine details from the sample inside container, especially in the presence of Opto-Fluidics.

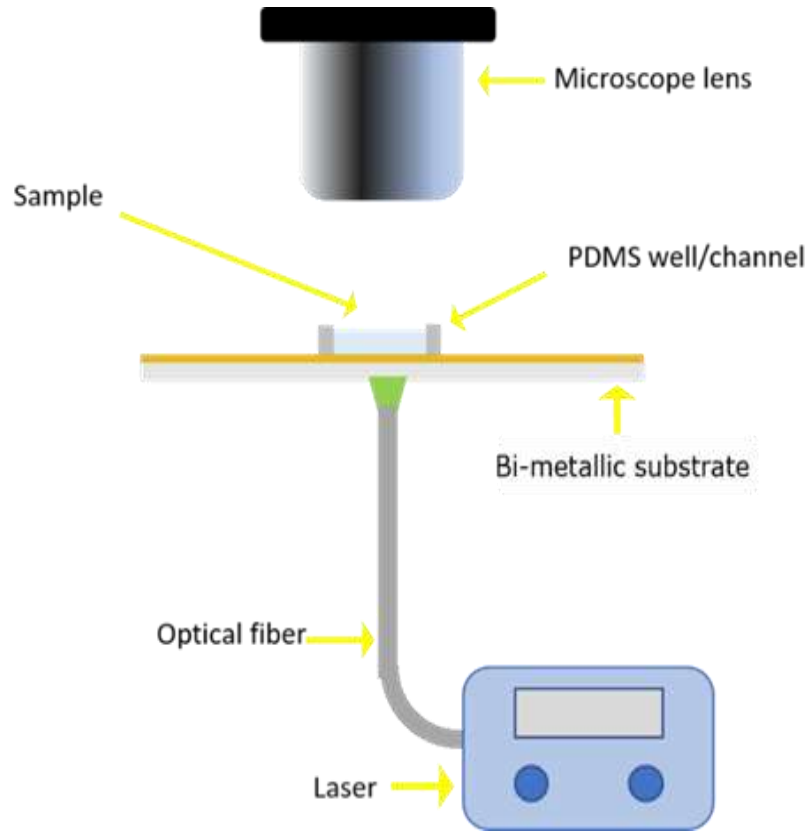


Figure 2.1 2-D schematic showing the experimental set-up. The optofluidic manipulation is controlled using a 532 nm laser shining from an optical fiber. The fluid sample is placed either in a PDMS well or PDMS microfluidic channel attached to plasmonic substrate. The substrate could be placed horizontally or be tilted using a special holder. When microfluidic channel is used, an external microfluidic pump can be connected to one end of the channel to introduce a continuous external flow.

2.1.1 Theoretical Simulations, Assumptions and Simplifications

All models used in simulation were initially designed in Solidworks 2019 as continuous objects, what allowed easier definition of domains and material specifications in COMSOL simulations. We used Thermo-Hydro-Mechanical module with the equations described below and all the parameters found in our previous study of plasmonic substrates including all the initial conditions for the temperature and all material properties.

For the symmetric horizontal and tilted substrate configurations the simulations were inside of circular wells with a radius of 2.5mm and height of 2mm. The configuration with additional flow was simulated in a section of a microfluidic channel with the dimensions 5x5x2mm. The nano-scale bi-metallic Cr-Au substrate was modeled using a thin layer approximation. Physical parameters of glass, water, gold, chromium and PDMS were taken from the COMSOL material library. No-slip boundary conditions were used in all simulations. Laser heating was approximated in a simplified way as uniform heating of a round spot on a substrate to the temperature $T = 303.15$ K, while the rest of the system was initially at ambient temperature of $T_{\text{ext}} = 293.15$ K.

2.1.2 Simulations of Fluid Mechanics

For each of the three models, the continuity equation for the conservation of mass and incompressible steady-state Navier Stokes equation for a single-phase fluid were used in the simulations.

$$\nabla \cdot (\rho \mathbf{u}) = 0 \quad (1)$$

$$\rho(\mathbf{u} \cdot \nabla) \mathbf{u} = \nabla * [p\mathbf{I} + \mathbf{k}] + \mathbf{F} + \rho \mathbf{g} \quad (2)$$

$$\text{Where: } \mathbf{k} = \mu(\nabla \mathbf{u} + (\nabla \mathbf{u})^T) - \frac{2}{3}\mu(\nabla \cdot \mathbf{u})\mathbf{I}$$

It was assumed that only density was temperature dependent and it was evaluated at the reference pressure $\rho = \rho(T, P_{\text{ref}})$.

2.1.3 Simulations of Heat Transfer

To simulate temperature distribution the following steady state energy balance equations for liquid heat transfer was used in the simulations:

$$\rho C_p \mathbf{u} \cdot \nabla T + \nabla \cdot \mathbf{q} = Q + Q_p + Q_{vd} \quad (3)$$

$$Q_p = \alpha_p T \left(\frac{\partial p}{\partial T} + \mathbf{u} \cdot \nabla p \right) \quad (4)$$

$$\alpha_p = -\frac{1}{\rho} \frac{\partial \rho}{\partial T} \quad (5)$$

$$Q_{vd} = \tau : \nabla \mathbf{u} \quad (6)$$

where ρ is density as a function of temperature and is also evaluated at the reference pressure, the specific heat capacity $C_p = 4179.6 \text{ J kg}^{-1} \text{ K}^{-1}$, \mathbf{q} is the heat flux by conduction, α_p is the coefficient of thermal expansion, Q_p is work as a result of pressure changes and Q_{vd} is the viscous dissipation in the fluid.

Conductive heat transfer between solids was simulated using following steady state equation for conductive heat transfer:

$$\rho C_p \mathbf{u} \cdot \nabla T + \nabla \cdot \mathbf{q} = Q + Q_{ted} \quad (8)$$

$$Q_{ted} = -\alpha T : \frac{dS}{dT} \quad (9)$$

where specific heat capacity is a function of the specific material, Q_{ted} accounts for thermoelastic damping and Q accounts for heating from other sources.

To reduce the computational cost of computing heat transfer in thin Cr-Au bi-layer, the Cr-Au layers were modeled with COMSOL's Thin Layer model using Thermally Thin Approximation.

This was described using following steady state heat equation for the thin layer approximation:

$$\nabla_t \cdot \mathbf{q}_s = d_s Q_s + q_0 \quad (10)$$

$$\mathbf{q}_s = -d_s k \nabla T \quad (11)$$

where d_s is the layer thickness, Q_s is density distributed in the layer, q_0 is the heat flux entering the layer and \mathbf{q}_s is Fourier's law describing heat leaving the layer.

2.2 Results of Simulations and Experiments

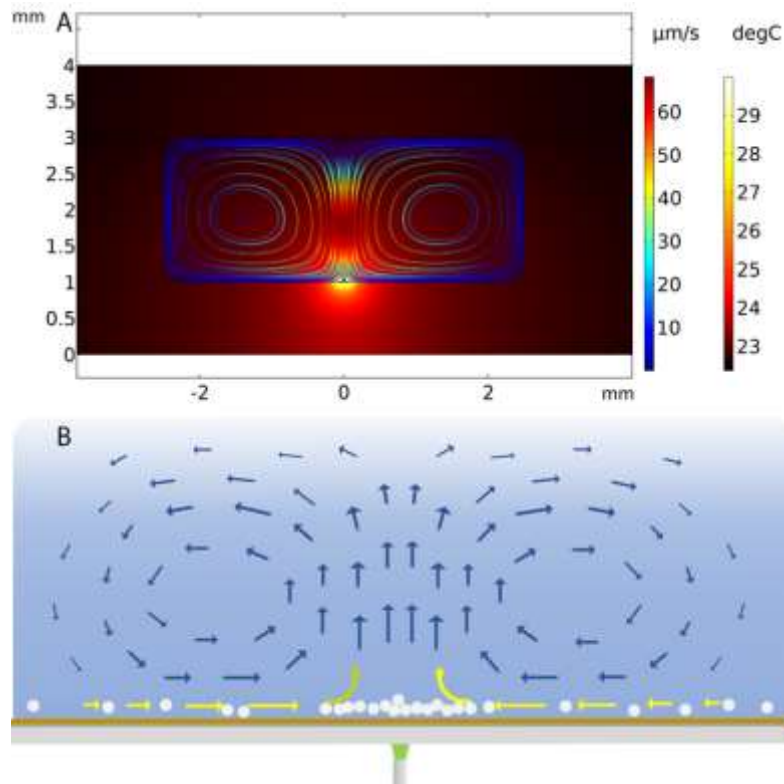


Figure 2.2 2-D cross-section of the simulated temperature distribution and the streamline plot of a fluid sample in a cylindrical well. The details of the current are shown in the bottom image. In the top image the streamlines are colored according to the fluid velocity (left color scale), and they are superimposed on a temperature map of the system (right color scale).

2.2.1 Horizontal Substrate without Additional Flow in Channel

Figure 2.2 shows simulations of cross-section of the temperature distribution in a circular well. The flow lines form symmetric loops. Overall, the current has a toroid shape. The bottom part of the Figure 2.2 shows the direction of the particle movement in such currents. The microbeads are moving towards the center of the toroid current and concentrate above the heated spot. This is experimentally demonstrated in Figure 2.3, where ~100 microbeads were captured above the heated spot.

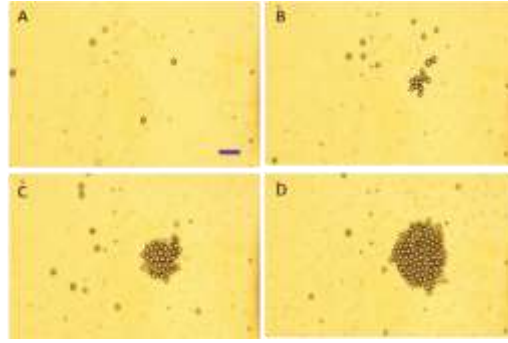


Figure 2.3 Images show particles manipulation in the cylindrical well. Particles are captured from the fluid sample above the heated spot for 5 minutes. Part A shows the original substrate and randomly distributed particles present in a low concentration in the fluid sample. After current is established, parts B-D consequently show growing number of particles. Part D shows approximately one hundred microbeads captured from the whole well and forming a single layer on the substrate. Pictures were taken under 10X magnification. Scale bar is 100 μm . The laser power was 30mW shining over a circular spot around 100 μm in diameter.

2.2.2 Microfluidic Channel with an External Flow

Many practical applications of microfluidics require isolation of particles or cells from fluid samples. However, to increase the processed sample volume the particle isolation has to be run continuously. This can be done by incorporating the particle isolation component into a microfluidic channel and simultaneously capture particles and pump in fresh fluid. This regime is simulated in COMSOL and demonstrated in Figure 2.4 Part A shows that the external flow in the microfluidic channel breaks the symmetry of the optofluidic current along the flow but preserves it perpendicular to the flow (Figure 2.4C). The loops tilt with the flow (Figure 2.4B), and as a result, particles are getting captured not above the heated spot, but down the flow. However, they are still captured at equal distance from the channel walls (Figure 2.4D). Figure 2.5 demonstrates the experimental particle capturing in a microfluidic channel with the external flow. The substrate used in the experiments intentionally has small holes, so the laser shining from above the substrate

can be located. It can be observed that after 5 min of operation a cluster of particles form, and the center of the cluster is shifted in the direction of the flow.

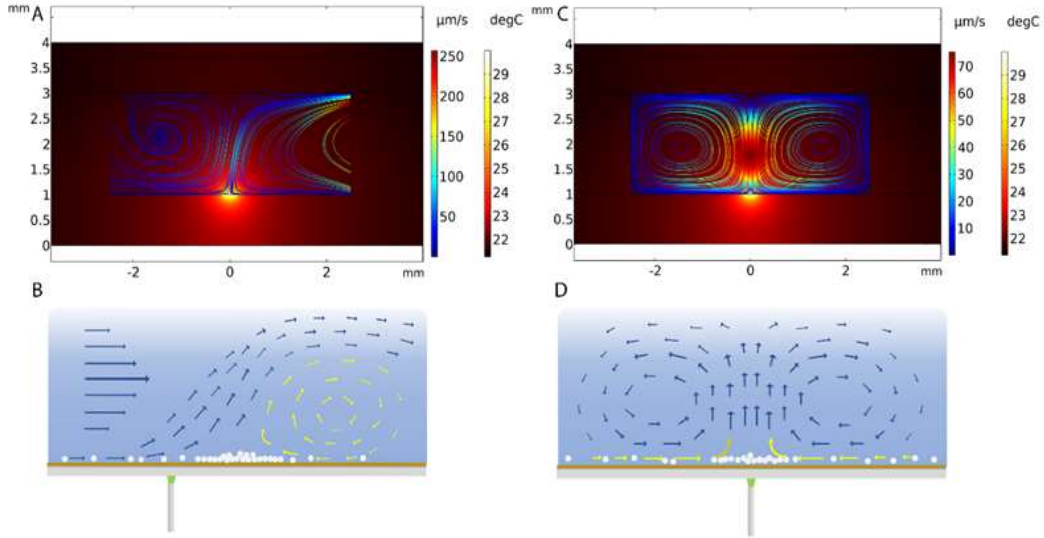


Figure 2.4 2-D cross-sectional temperature and velocity streamline plots for fluid flowing through the channel on the XZ and YZ planes (along and across the flow). Part A shows the fluid streamlines through the channel along the XZ plane. Part B illustrates captured particles onto the substrate at a location shifted in the direction of the external flow relative to the heated spot. Part C demonstrates the convective vortices on the YZ plane perpendicular to the direction of flow and Part D shows that the particle accumulation is in the middle of the channel at equal distance from the walls.

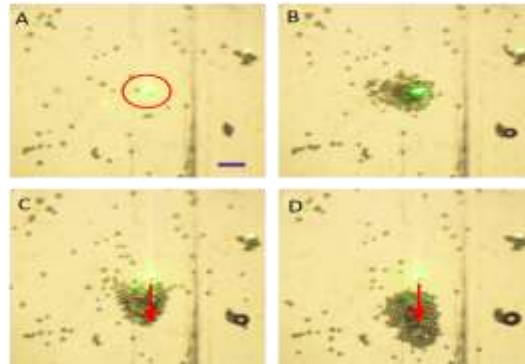


Figure 2.5 Images show particles manipulation in the channel with external flow. The red circle in part A shows location of the laser spot, which would be an aggregation center of the particles in absence of flow (B). Red arrows in image C and D show the direction of continuous flow. It can be noticed that the center of particle accumulation is down the flow. The experiment continued for 5 minutes. The flow rate was set at 10 $\mu\text{l}/\text{min}$ and the laser power intensity was 30mW. Scale bar is 100 μm .

Figure 2.6 shows that the particle capturing is greatly affected by the velocity of the external flow. For very low velocities ($0.1 \mu\text{m/s}$, Figure 2.6A) slow the optically generated toroid current is not disturbed. When the external fluid velocity increases to $10 \mu\text{m/s}$ (Figure 2.6B), the loops of the toroid current are tilted and the area for capturing beads is further down the stream (similar to what is observed in Figure 2.4A). Finally, for even faster external currents ($100 \mu\text{m/s}$, Figure 2.6C), the loops disappear and the only featured related to Opto-Fluidics is bending some of the flow lines. This set of simulations clearly reveal the impact of external flow with different velocity on the convective currents within Opto-Fluidics. When we need to isolate particles or cells from fluid samples in future experiments, one of the priorities of experiment will be identifying an appropriate velocity of the external flow, that allows Opto-Fluidic currents to capture particles and an increase of the processed sample volume.

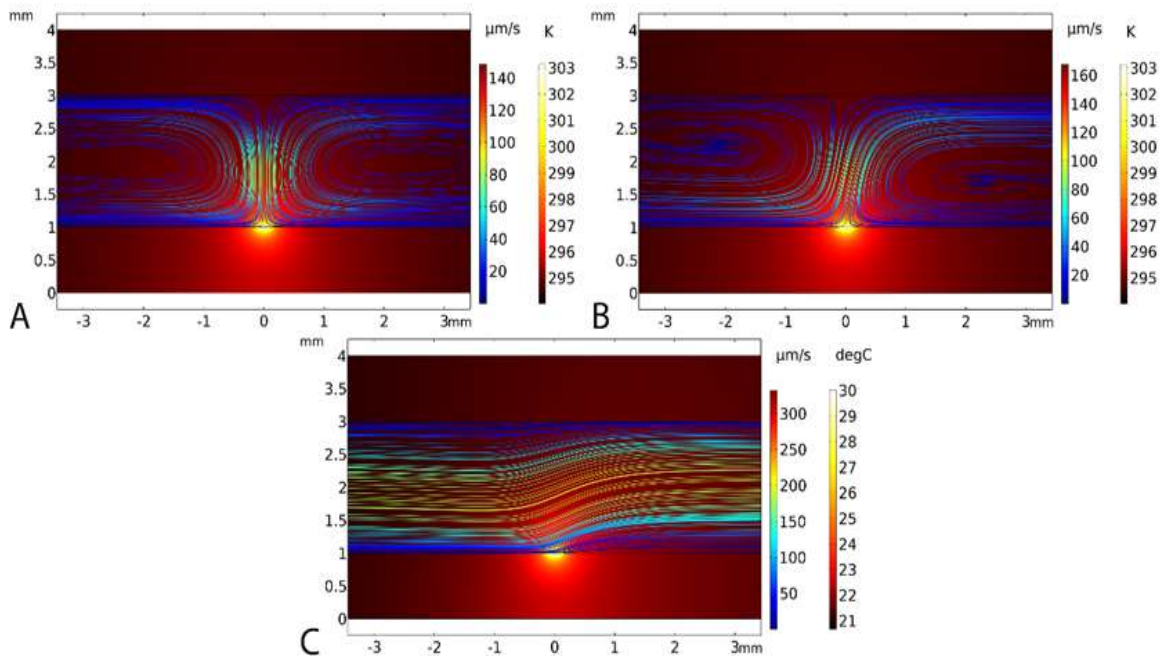


Figure 2.6 Change in the microfluidic flow pattern depending on the laminar flow introduced at the channel input. A) The flow is very slow ($0.1 \mu\text{m/s}$), so the toroid pattern is not disturbed. B) The flow is stronger ($10 \mu\text{m/s}$), so loops are tilted and the area for capturing beads is further down the stream. C) The strongest flow ($100 \mu\text{m/s}$) breaks the loops, and the only featured related to optofluidics is bending some of the flow lines.

2.2.3 Tilted Microfluidic Channel without an External Flow

The third optofluidic regime with a tilted microfluidic channel without external flow can be used for better understanding of optimal operation conditions for efficient particle capturing. While operation of microfluidic channel at small (less than 10°) angle to the surface would not produce significant changes, larger tilts might greatly change the optofluidic flow and affect particle manipulation. Figure 2.7 demonstrates that the toroid pattern is disrupted along one of the directions when tilt is introduced (Figure 2.7A). The particle deposition becomes non-symmetric (Figure 2.7B) in that direction. In the perpendicular direction, both the flow and the particle deposition are still symmetric (Figure 2.7C, D). Figure 2.8 shows experimental confirmation of the simulations. The particle deposition on the tilted substrate is not symmetric, and the higher portion of the substrate has more articles deposited, consistent with the prediction from Figure 2.7.

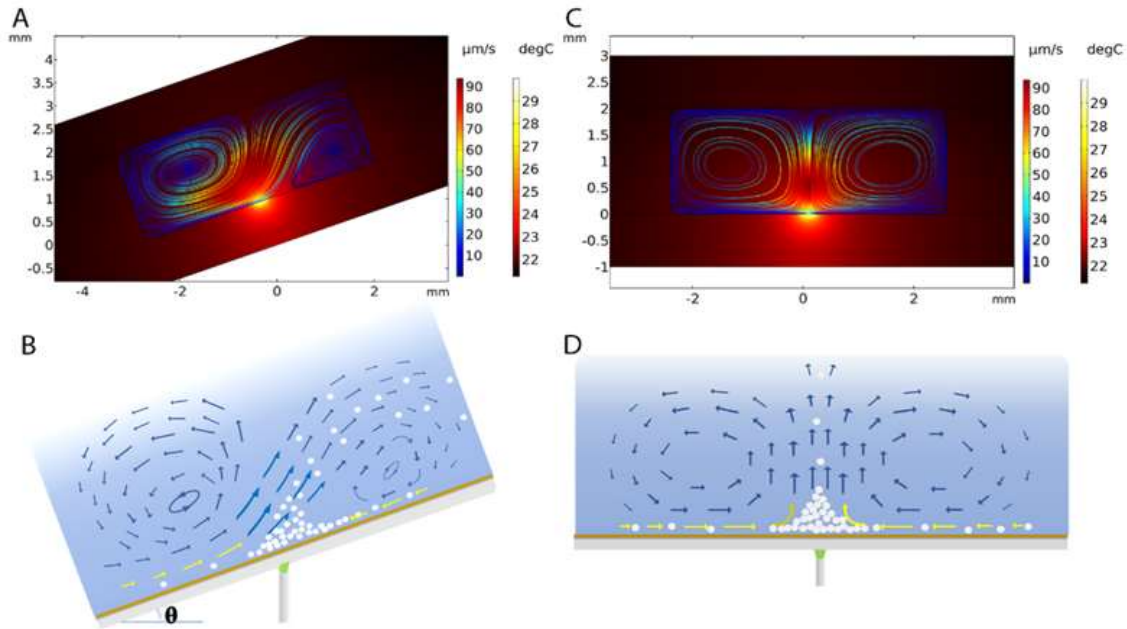


Figure 2.7 2-D cross-sectional temperature and velocity streamline plots of the channel tilted at 20° relative to the horizontal level. Part A plots fluid streamlines and the development of vortices along the plane of rotation. Part B illustrates non-symmetric accumulation of particles. Part C shows the rotational streamlines perpendicular to the flow shown in Image A. Part D illustrates symmetrical deposition of the beads in the cross-section corresponding to Part C.

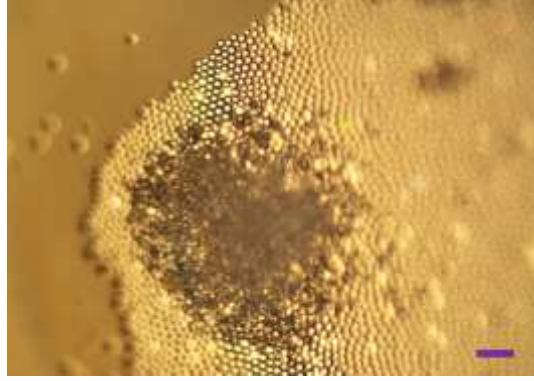


Figure 2.8 A 10X magnification microscopic image showing the microparticles aggregation on an inclined substrate. Both left and right parts of this image are slightly out of focus because of the tilt of the substrate. More microparticles were aggregated on the right (higher part of the substrate). Scale bar is 100 μ m, laser power was 50 mW, angle is 20 degrees.

2.3 Conclusion

In this chapter, we theoretically predicted and experimentally demonstrated that three different regimes of Opto-Fluidics produce different convective flow patterns and differently accumulate particles. These results are important for better understanding of design principles for practical applications needing particle manipulation. The simulations and the experiments confirmed that optofluidic particle capturing can be conducted even in a microfluidic channel continuously pumping fresh fluid. In addition to that, it was shown, that proper placement of the substrate is important for consistent operation since significant tilts result in different distribution of particles on the surface. This research lays foundation for new practical optofluidic systems integrated with microfluidics. They can be used for continuous concentration and capturing of cells and/or bacteria from different biological samples.

Chapter 3: Microparticles Manipulation by Using Opto-Fluidic Chip

In previous chapters, we identify the optimal thermal-plasmonic(metallic) structure that can be used for assembling Opto-Fluidic chip. This chip can effectively concentrate and capture microparticles inside the liquid sample by using innovative OFM technology. The COMSOL simulations can uncover the 3D patterns of convective flows in Opto-Fluidics. Additionally, simulations can also predict the changes of convective flow patterns in Opto-Fluidics corresponding to the change of initial condition setting. These works can help us clear the thoughts about how to use the Opto-Fluidic chip to isolate microparticle from samples. Meanwhile, to separate a certain type of microparticles from liquid sample normally relies on well-established conventional approaches. Popular approaches such as filtration and centrifugation, are widely applied based on their popularity of devices. The filtration technique can be categorized into multiple types that base on the diameters of particles being filtered. Filtration types such as microfiltration, ultrafiltration, nanofiltration and reverse osmosis are commonly used in variety of fields. The biggest difference among them is the size of filtered microparticles, which can vary from 1000 microns to 0.1 nanometer [39]. The centrifugation technique obeys the sedimentation principle. Under the effect of super centrifugal force, microparticles can form sediment layers at the direction of centrifugal force. When either approach is used for processing biological samples, we want the desired objects are isolated from the sample, then conduct subsequent analysis on the captured particles. Whereas, either filtration or centrifugation is used to isolate particles from sample, it can bring difficulty on the collection of desired particles. For instance, after

centrifugation, the desired particles can form a layer of sediment at the bottom of sample. To collect these particles, it usually requires manual operation to remove the supernatant and collecting pellet. Meanwhile, centrifugation is unlikely to handle small volume sample with a couple of microliters. On the other hand, if we use filtration technique to process sample, then how to remove desired particles from the filter membrane becomes a knotty task, let alone to collect the particles for subsequent tests.

As mentioned earlier, our chip consists of a PDMS mold and a plasmonic substrate. The PDMS mold is designed to contain samples on top of substrate. The PDMS mold can be made with different structures, such as microfluidic channel or cylinder shape micro-reservoirs. Either soft lithography or mold casting technique can be used for embedding the structure into PDMS mold. Next, attach the PDMS mold onto substrate to form a permanent bonding. Then we get an Opto-Fluidic chip. One type of Opto-Fluidic chip has cylinder shape micro-reservoirs can be used to process small volume of samples. Another type of chip has microfluidic channel, that allows sample flow across the space of channel and bring in Opto-Fluidic in the meantime. The second type of Opto-Fluidic chip can process more samples per unit time. That is because the microfluidic channel allows Opto-Fluidic to process flowing samples. This design can push the sample processing power of the chip to a new level. Meanwhile, the key feature of microfluidic channel is structural miniaturization. It mainly consists of wispy channels and it allows a very small amount of sample run through per unit time. The dimension of channel varies typically from tens to thousands of micrometers. The benchmark of microfluidic channel fabrication process has been established back to 1990s [40]. There are plenty of researches that focus on developing various type of microfluidic system to fulfill specific tasks. Taking microfluidic system as a platform for

separating particles from fluids is one of many applications. Many particle separation techniques that rely on microfluidic system have been developed in this promising subject.

According to the mechanism of separation, microfluidic devices can be classified into three categories, which are passive devices, active devices, and integrated devices [41]. The microfluidic channels in some passive devices contain indented, protruded, or curved sidewalls to direct particles. Other passive devices consist of repeated geometric patterns within the flow cavity of the microfluidic devices. Another type in passive devices contains adhesion sites to promote particle attachment or temporary adhesion. For the active devices, researchers mainly apply controllable forces, such as electric forces, magnetic forces, acoustic forces, and optical forces to manipulate the movement of particles, in order to achieve specific goals, such as particle separation and sorting. Integrated devices are those that adopt more than one method for manipulating particles in microfluidics systems. Such integrated devices combine active and passive components to conduct isolation, sorting and other delicate tasks [41]. The Opto-Fluidic chip with microfluidic channel structures can be classified into the category of active device.

In conclusion, when conventional methods such as centrifugation, filtration and flow cytometry have fallen short on what researchers desperately sought for, particle separation techniques that rely on microfluidic system can be a good alternative. In this chapter, we will demonstrate that the Opto-Fluidics chip can concentrate, isolate, and collect microparticles from both static sample and fluid. Meanwhile, the chip can process small volume of sample and remain a capability of processing fluid sample rapidly.

3.1 Methods and Experiment Results

To concentrate and collect the microparticles from original sample, we need to build up a controllable flow system that can connect with Opto-Fluidics chip. This system basically consists

of Opto-Fluidics chip, microfluidic Tubing, ultra-thin syringe needle, and microfluidic pumps. We use these components to assemble a system which can create sample flows inside Opto-Fluidic chip. The Figure 3.1A at below clearly indicates each component in system. The Figure 3.1B shows the Opto-Fluidic chip is placed under microscope lens in experiment. In this way, we can observe Opto-Fluidic manipulation over particles in real time. The entire process of particle manipulations includes concentrating and removing from chip, both take place inside the chip and can be observed under microscopic lens. A picture of Opto-Fluidics chip with microfluidic channel structure is shown as Figure 3.1C.

To better explain how this flow system works with Opto-Fluidic chip in order to enable the chip process fluid sample, a 2D sketch of the entire set up is given as Figure 3.2 Furthermore, another 2D sketch which shows fine details of Opto-Fluidic chip from top view is given as Figure 3.3. Both the concentrating and capturing of particles from sample flow will be taken place inside the microfluidic channel space, which is denoted in Figure 3.3.

Before we start the experiment, sample is stored in a syringe, which is controlled by one microfluidic pump (Figure 3.1A. a). This pump can slowly squeeze syringe to inject samples into the system. The injected sample flow can go through microfluidic tubing which connects syringe and chip, then gets into the channel inside chip. The Opto-Fluidics will be generated inside channel space of chip when laser beam strikes from below, onto the plasmonic structure covered area (Figure 3.1A i). Shortly, microparticles inside channel space can be manipulated by Opto-Fluidics and end up forming an aggregation around the spot where laser beam strikes. Once the microparticle concentrating is completed, we can capture and remove the aggregation from where it formed. Therefore, another microfluidic pump (Figure 3.1A b) is required for the second step of manipulation. The second pump is used to generate attraction force to remove aggregated particles

from chip. This pump connects with the syringe needle (Figure 3.1A I) through microfluidic tubing. Consequently, the influenced area of suction force is constrained nearby the tip of syringe needle. By setting the aggregating center close to syringe tip in advance, the aggregated microparticles can be sucked into the needle. We halt the pump as soon as particles aggregation is completely removed. Meanwhile, the collected particles will stay inside the syringe needle. Then, the syringe needle can be detached from the Opto-Fluidic chip. The captured microparticles that are contained inside needle can be easily released onto a different place for taking further analysis.

In this chapter, our experimental results can demonstrate the capability of Opto-Fluidic chip. We use polystyrene microbeads mixed with water to get the particles suspension, which as the sample used in experiments. Tests on the Opto-Fluidic chip by using microparticles with different size can demonstrate the range of size of objects that can be manipulated by Opto-Fluidics. The successful collection of particles from static liquid sample and from sample flow, and selectively collect one type of particle from the mixture of particles with different size can prove the capability of this system. Meanwhile, the entire manipulation process that takes place inside the Opto-Fluidic chip can be monitored by optical microscopy in real time. This fact allows us to timely adjust every experimental parameter accordingly to achieve optimal outcomes on particle's concentrating, isolating, and sorting respectively.

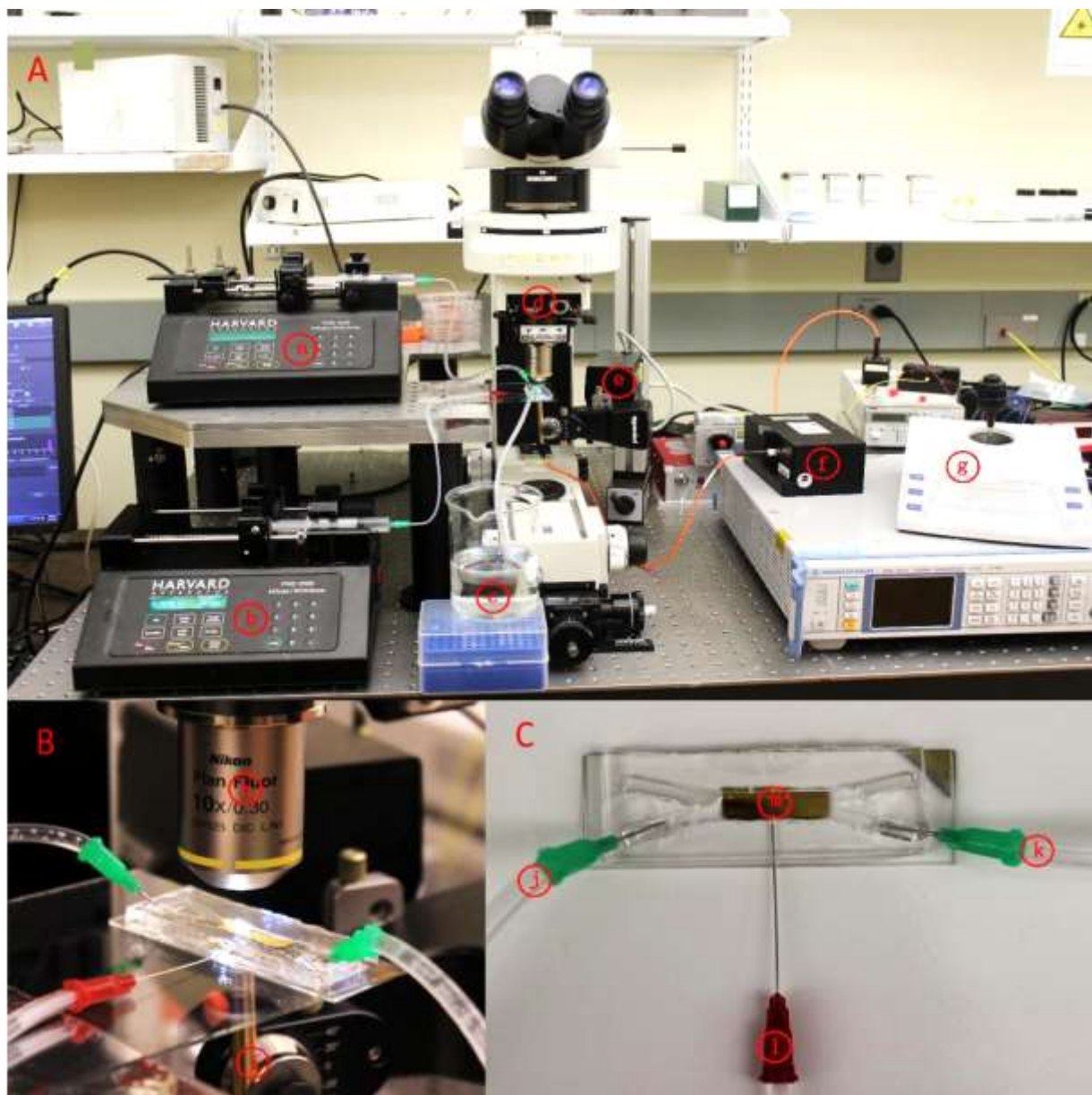


Figure 3.1 Pictures present the complete experimental set-up. (a) and (b) are two pumps that are used to inject liquid samples and remove particle aggregation from channel. (c) is a waste container. (d) is a microscope that enables us to watch procedure in real time. (e) is manipulator arm that holds the part (i). (f) is the laser generator that connects (i) via optical fiber. (g) is the controller of (e). Figure 3.1B shows the way we set the Opto-Fluidic chip in the system. (h) is a 10X microscope lens. (i) is the fiber chuck and holder made of copper. An optical fiber is inside the chuck. Figure 3.1C gives closer look at chip. (j) and (k) as the main inlet and outlet of the chip. (l) as the secondary outlet, for collecting the aggregated particles from the sample. (m) is the main chamber of microfluidics channel and is also where the opto-fluidics manipulation occurs.

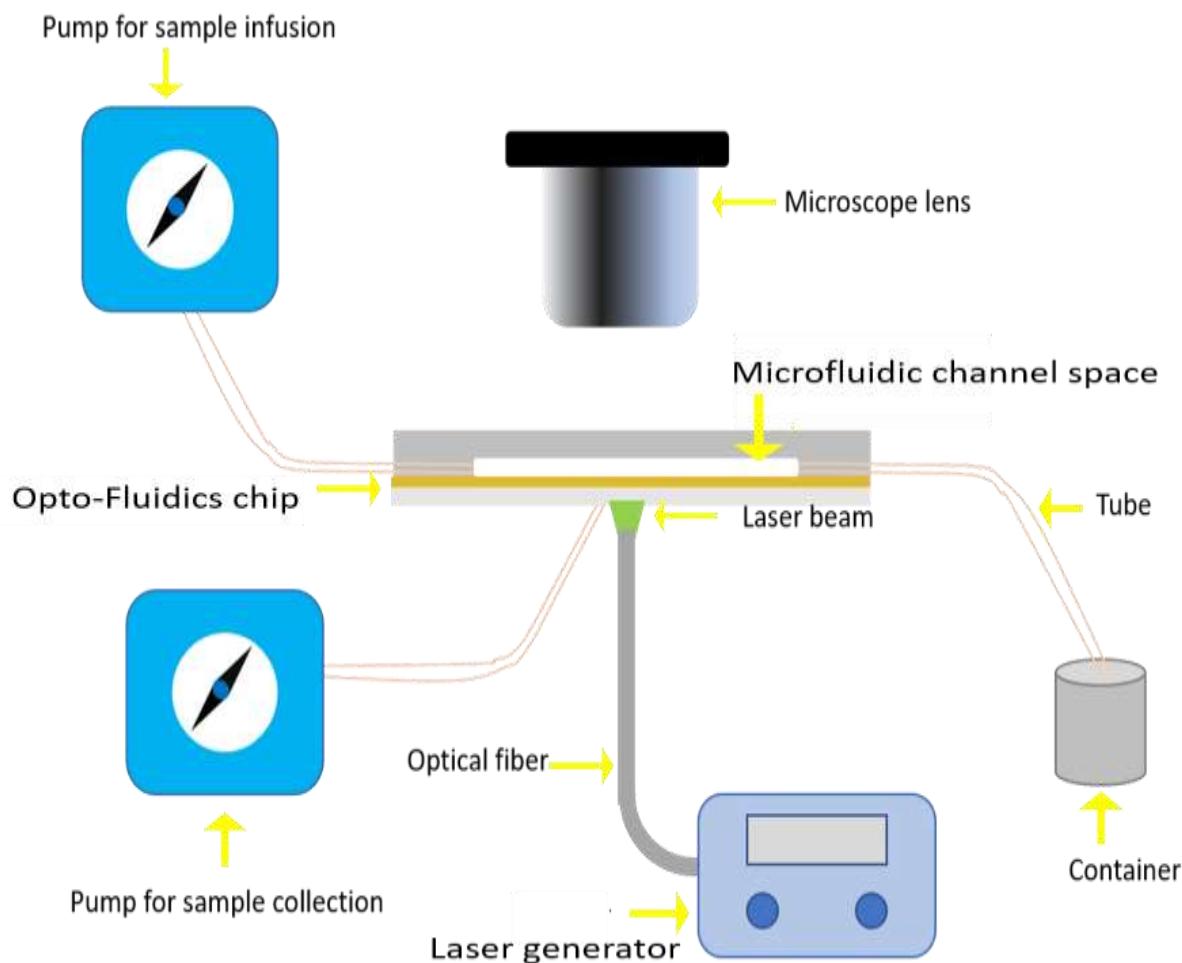


Figure 3.2 2-D sketch of the experimental set-up. It clearly denotes all essential components. The pump on the top left injects the sample into the system. Sample fills out the microfluidic channel space inside chip. Only sample inside the space will be affected by Opto-Fluidics. The pump at bottom left is used for generating suction force. This force can be used for removing aggregated particles from channel space. Treated samples will get into the waste container. One end of the optical fiber is connected to the 532nm laser generator, while the other end points to the bottom surface of the chip perpendicularly.

For all experiments in this chapter, we use water as the medium and add polystyrene microbeads in water to make beads suspension as sample. The concentration of particles in water is well controlled. To determine an appropriate concentration, we can observe sample using 10X magnification microscope lens. It is good if we see countable particles in view. Over dense particles in view makes particle concentration useless. Over-diluted sample can take more time to form a noticeable aggregation.

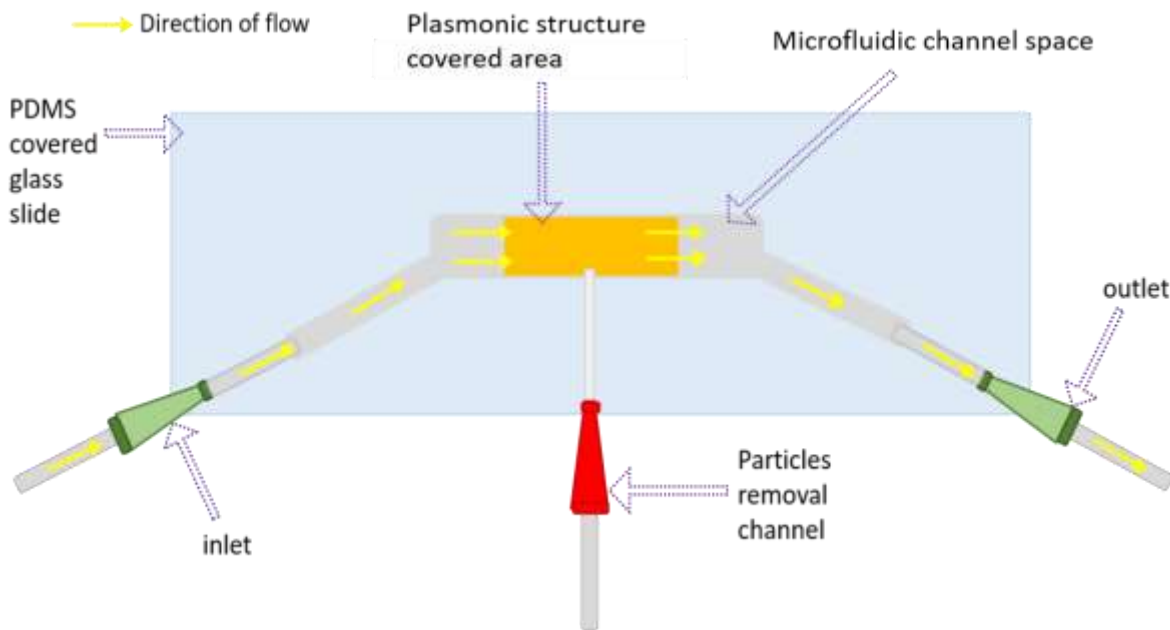


Figure 3.3 2-D sketch of Opto-Fluidic chip from the top view. The yellow arrows represent the direction of sample flow inside channel. The orange color square represents plasmonic substrate. Three syringe needles built in the chip, connect the channel space with tubing. The intersection surface of the channel is rectangle, which has 2 mm height and 6 mm width. The length of the plasmonic substrate area is 25 mm.

Basic steps of doing experiments in this chapter are similar. First, we use the system to capture particles from standing liquid sample. Turn on microfluidic pump to infuse the beads suspension into the channel through inlet, until the channel space is filled up completely. Then stop the pump, turn on laser generation and use OFM to form particle aggregation at the heat spot. The location of heat spot is set very close to the tip of needle. This syringe needle is used for collecting aggregation. Normally, the distance between the heat spot center and the tip of syringe needle is no more than 500-micron in experiments, to make sure particle aggregation is under influence of suction force. Shortly, we notice the particle aggregation stop growing. This means there are very few free particles are left in the effective range of Opto-Fluidics. Then, we turn on the second pump which connects to the syringe needle (needle in color red in Figure 3.3) for collection. This pump generates suction force round the tip of needle. Consequently, the beads aggregation is

sucked into syringe needle. In this way, the Opto-Fluidic chip can process sample in batches. Based on previous simulation results, effective range of Opto-Fluidics only inside the main fluidic channel space. (channel dimension: H 2mm * W 5mm * L 20mm). As conclusion, chip can process 200 ul sample per batch.

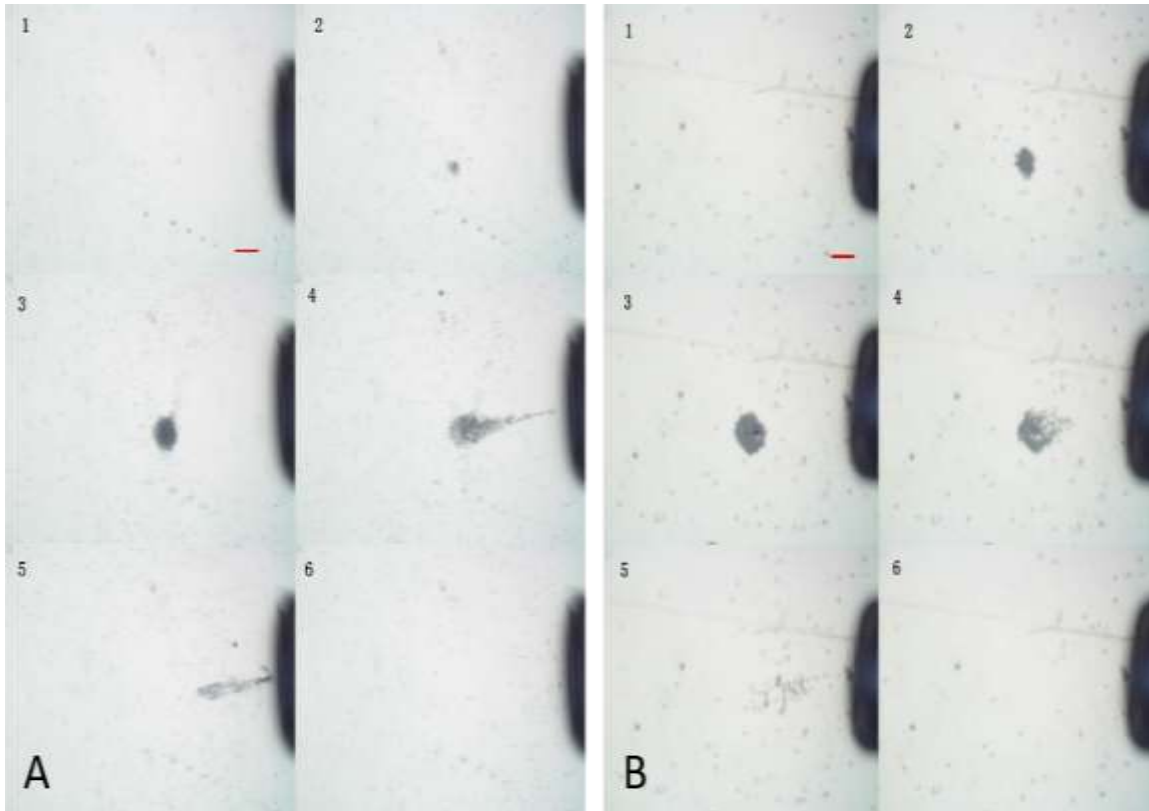


Figure 3.4 Two sets of images show 5-micron and 10-micron particles manipulations. Each set includes 6 images. The images from left set show the consecutive process of 5-micron diameter particles being concentrated(A1-A3), and be completely removed (A4-A6) through syringe needle. The needle tip is the black prominence on the right side of each image. Images are taken under 10X magnification. 100 µm scale bar in color red is given at the right bottom corner of image 1. Images from right set show a same process on 10-micron particles. Laser power applied for 5-micron particle (10 mW) concentration is lower than 10-micron particle (20mW).

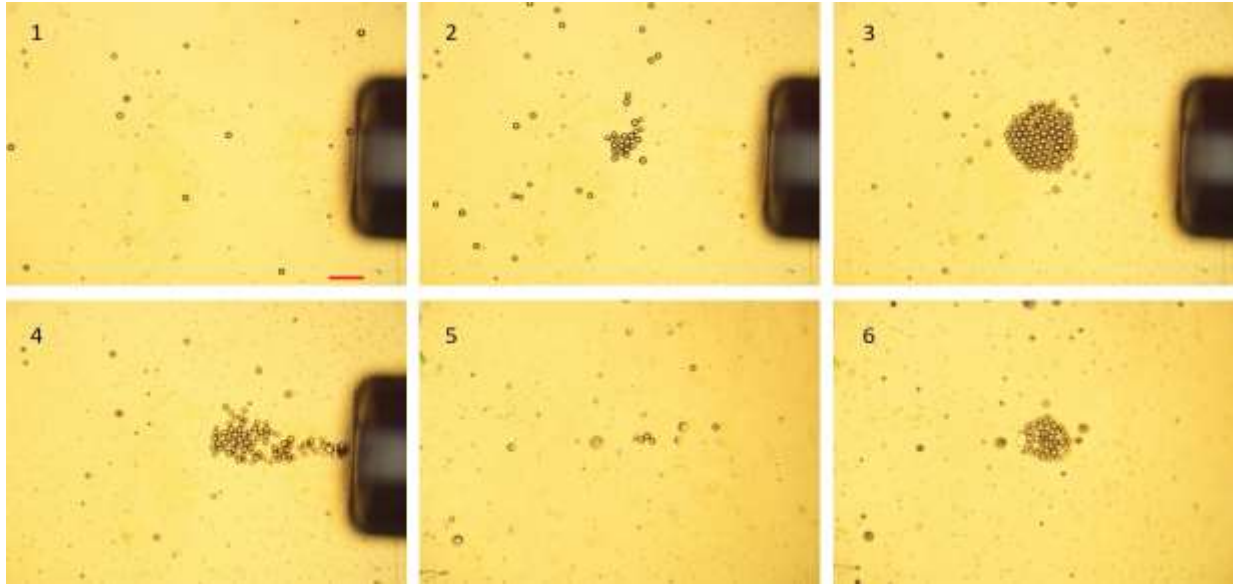


Figure 3.5 Images show the 20-micron particles manipulation. 10X magnification was applied. 100 μm scale bar in color red is given at the right bottom corner of image 1. The six images in this figure respectively represent (1) the original condition, (2) concentration of particles, (3) aggregation formation, (4) collection of particle through needle, (5) collected sample is released from needle onto new slide and (6) reaggregated particles. Laser power is 30 mW.

Since this system enable to concentrate and capture particles from sample, it is also important to know the proportion of particles that can be successfully transferred among all captured particles. This proportion represents the recovery rate of the Opto-Fluidic system. We know that the loss of particles in the middle of transferring process is inevitable. The recovery rate can be an indicator shows the efficiency of capturing by the system to some extent. In order to know the recovery rate, we need to count the total number of beads which are concentrated by Opto-Fluidics. Therefore, we use the 20-micron beads to replace 10 and 5-micron beads, to get a better vision for beads counting. After the bead's aggregation is completely collected by needle, the following steps are:

1. Stop pump, remove the needle from chip.
2. Captured beads are stored inside the needle, get released onto a new Opto-Fluidic chip with micro-reservoir structure.
3. There always be a small amount water captured by needle along with particles. So, use Opto-Fluidics to re-concentrate all particles that in transferred sample. By this way, we can calculate the recovery rate via counting

the total amount of beads from both image 3 and image 6 (Figure 3.5). Fortunately, the 20-micron beads aggregation can be formed in single layer structure, makes the counting work feasible. The total number of beads in aggregation is about 95, counted base on image 3. The total number of beads in aggregation is about 47, counted base on image 6. Therefore, to get the recovery rate, use 47 divided by 95, which leads to nearly 50%.

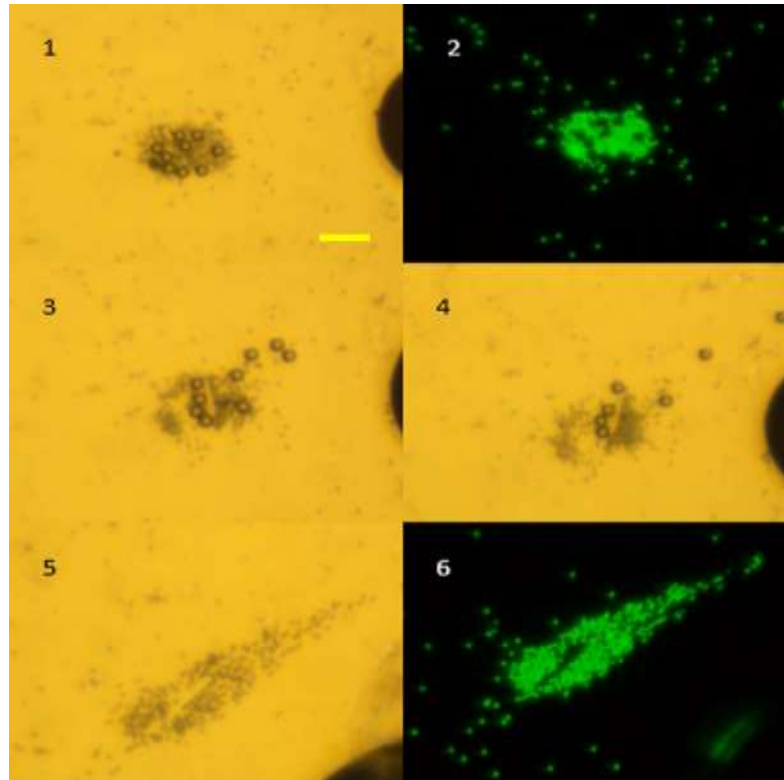


Figure 3.6 Images shows the separation of two types particles (5-micron and 20 micron) from a mixed particles aggregation via using the system. 10X magnification was applied. The 5-micron beads can emit green light under blue excitation light (465 nm - 495 nm). Image 1 is under bright field and 2 is the corresponding fluorescence image. Same principle for image 5 and 6. The black prominence at the right edge of each image is the tip of needle. 100- μ m scale bar in color yellow is given at the right bottom corner of image 1.

A tentative test on system for the particles sorting base on size is presented in Figure 3.6 At the beginning of this experiment, we find out a suitable power range for generating Opto-Fluidics which can concentrate both size of particles and form a mixed aggregation. The power of laser is set around 15 milliwatt. As we expected, the 5-micron beads can aggregate in a faster rate than the

20-micron beads. Let the Opto-Fluidic keeps working until the aggregation stop growing. Then we use the pump to create suction force at the tip of syringe needle. The particle aggregation located next to the needle tip, can be affected by the suction force. However, by setting the strength of suction force at a moderate level (15 ul/min), only the 20-micron size beads can be removed from the aggregation. Meanwhile, most 5-micron size beads in aggregation remain still. Image 1 shows beads with different sizes are aggregated at heat spot. Image 2 clearly shows the 5-micron beads emit green fluorescence under excitation light while the 20-micron beads are not fluorescent. The reason for using fluorescent beads mixed with non-fluorescent beads is to have a better view on the separation of two types of beads, and to easily identify out the positions of smaller particles in mixture. Image 3 and 4 show the separation of two sizes of particles when apply a suction force to the aggregation. The 20-micron beads can immediately respond to the force and get collected by the syringe needle. Meanwhile, most of the 5-micron beads remain in situ. Shortly, all 20-micron beads are gone (see Image 5) while 5-micron beads aggregation are left behind. The shape of 5-micron beads aggregation is deformed, showing comet tail pattern. This is because the particles' collision happened when 20-micron beads get capturing, while some 5-micron beads are pushed towards the needle by the 20-micron ones. More specifically, the 5-micron beads can also be impacted by the suction force. But their moving speed is much slower than the 20-micron beads. That is why we can observe a clean separation of two types of beads, and the 5-micron beads aggregation in shape of comet's tail. If we turn off the pump and allow Opto-Fluidics work for a couple minutes, the shape of 5-micron beads aggregation can become circular again. The good explanation for the different reactions to suction force from 5- & 20-micron beads is that the suction flow created by the needle does not closely attach to the bottom surface of channel. This is because the wall thickness of syringe needle is bigger than the diameter of smaller beads.

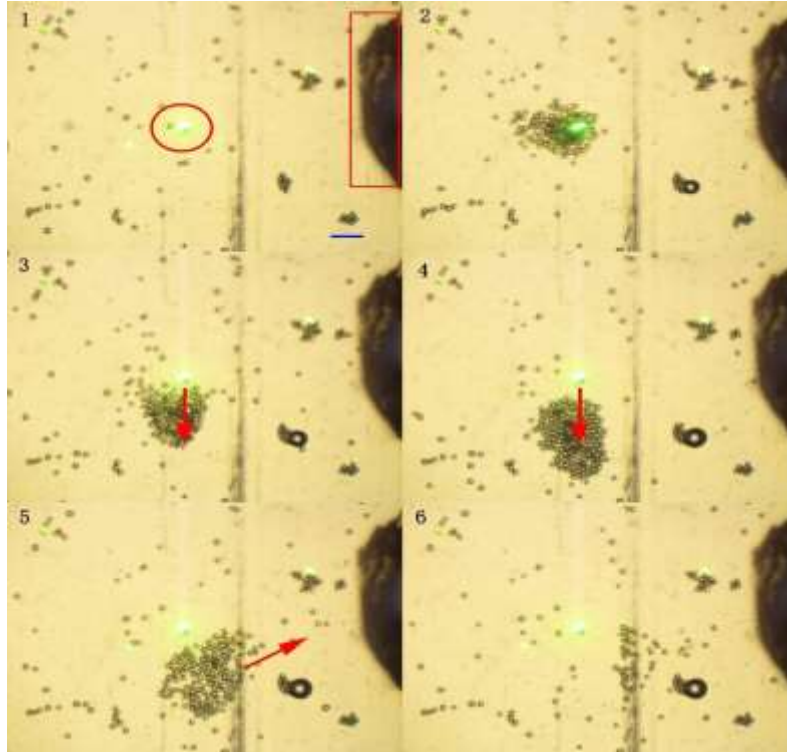


Figure 3.7 Images shows the capturing particles by using needle from flowing sample. Image from 1 to 6 show the process of beads aggregated and be captured through the syringe needle, which is the black prominence at the right edge of each image. The red circle in image 1 points out the laser spot, which is also the center of heat. Red arrows show the direction of shift of beads aggregation within flow. The 100 μm scale bar in color blue is presented at the right bottom of image 1.

Next, we introduce flow into Opto-Fluidic chip and want to figure out if particles aggregation still exists and can be captured. First, we set the flow rate as 5 ul/min at sample injecting pump, which means there are 5 ul new sample are pumped into the channel space in every minute. Image shows the direction of flow is downward. Under this rate, the Opto-Fluidics can still concentrate 20-micron particles and form an aggregation around heat spot (red circled in image 1). When we increase the flow rate up to 15 ul/min , we observe that particles aggregation as a whole piece shifts in the direction of flow. Image 3 and 4 clearly show the aggregation shifts, which is indicated by the red arrow. Meanwhile, the aggregation keeps growing in the presence of Opto-Fluidics, that makes the size of aggregation larger. Eventually, the aggregation stays still at the spot which is

pointed by the red arrow in image 4. By far, we can conclude that a small external flow (<10 ul/min) added on Opto-Fluidics can barely cause influence on particle aggregating. While the Opto-Fluidics can be affected by a stronger flow (>10 ul/min and <20 ul/min), and the center of aggregating can slightly shift in the direction of flow. The shifting will not stop if the flow is too fast (>25 ul/min) and eventually lead to the failure of particle concentrating. Simulations (Figure 2.6) show the shape of Opto-Fluidics in the presence of external flow with different flow rate. They can help to visualize the changes of composite flows. After we see a stable aggregation formed inside flow, we can use syringe needle (shown in red rectangular box in image 1) to capture the aggregation. Image 5 and 6 show the process of collecting particles from fluid.

3.2 Conclusion and Discussion

Experiments from the previous chapters have demonstrated that the Opto-Fluidic chip can concentrate microparticles in both static liquid sample and sample flow. In this chapter, an Opto-Fluidic system is built by using the chip and other auxiliary equipment. This system can process samples in batches if there is no continuous flow. Without additional flow, the 5-micron particles in sample can be concentrated and removed by the system. Similar operations can be completed by using either 10-micron particle suspension and 20-micron particles suspension. Furthermore, via the test using 20-micron particles, we figure out the particles which can be successfully transferred take up around 50% among all particles which are concentrated in the first step. This system can also exclusively collect the 20-micron particles from a mixed type particles aggregation. More importantly, this system can capture the particle aggregation as long as the injecting flow does not interrupt the concentrating process created by Opto-Fluidics. At last, the Opto-Fluidic chip is reusable, and the entire system is easy to assemble and maintain.

Chapter 4: Biocompatibility Test of Opto-Fluidic Chip

In previous tests, the experiment samples been used are the particles suspension. It can be prepared by mixing the polystyrene microbeads with water. These microbeads are indicators that can depict the patterns of convective flows inside Opto-Fluidics. More importantly, it is a direct demonstration that how the movement of microparticles can be manipulated by Opto-Fluidics. Previous experiment results also demonstrate that the Opto-Fluidic chip and the entire system built around it can concentrate, capture, and transfer particles from both static liquid samples and sample flow. So, in our next step, we want to demonstrate that cells in bio-samples, can be concentrated, captured, and transferred by using Opto-Fluidic chip, same as it did on polystyrene beads. However, before we use the chip to manipulate cells in bio-sample, we first need to demonstrate that cells can endure the Opto-Fluidic manipulation inside the chip, and the cells can remain normal and unharmed in the meantime.

4.1 Methods and Experiment Results

Before the experiments start, we need to conduct an analysis about which specific part of the Opto-Fluidic system may cause potential harms to cells. The three syringe needles embedded in chip (Figure 3.3) are portals for doing sample loading, drainage and collecting particles. The microtubing are used to connect microfluidic pump with syringe needles. These two parts can have direct contact with the sample, are normally cause no damage to cells. That is because both parts are standard medical supply in clinical. Meanwhile, the Opto-Fluidic chip is completely designed and fabricated in lab, has direct contact with bio-samples in experiments. It is the place where the

particles being concentrated and captured. It is possible that these manipulations upon cells can incur potential damages to cells. When we use polystyrene microbeads in experiments, we can see that most microbeads in suspension will settle down on the bottom surface after the sample was injected into chip. That is because the density of polystyrene beads is higher than water. Same situation will repeat on cells because most cells have a higher density than water. After the bio-samples get injected into the chip, cells will settle down and have direct contact with the thermal-plasmonic (metallic) substrate and with PDMS. Meanwhile, laser beam strikes on the substrate and cause local heat on the metallic surface. Therefore, the possible leading factor that can impact cell viability is heat.

The original design of biocompatibility test is to conduct the test on Opto-Fluidic chips which has microfluidic channel structure. However, some damages on cell may not lead to immediate cell death. Some damages on cells can present long term effects after incubating cells for some time. Cells can be dead or have abnormal growth after incubation. Meanwhile, unharmed cells can keep a normal cellular morphology, which is an important indicator. Therefore, we decide to use another Opto-Fluidic chip which has multiple cylinder shape reservoirs (Figure 4.1). This type of chip can contain cell samples in each reservoir and allows the sample does gas exchange with environment. This is important for doing cell culturing in situ at where cells have been treated by Opto-Fluidics. When we look into this chip, there are multiple wells on PDMS mold. In the corresponding positions, there are circular areas of metallic structure on glass slide. Each circular area has thermal-plasmonic structure and the diameter of area is same as the well. After giving a special treatment on contact surfaces, we attach the PDMS mold to the slide. The binding between glass and PDMS is strong and permanent. As a result, every well is insulated and leakage free. This chip allows us to generate Opto-Fluidics inside each well when well is filled up by bio-

samples. Furthermore, the multiple wells structure on Opto-Fluidic chip can do multiple tests. At different well. We can set different laser powers on different well and identify the possible reactions of cells to Opto-Fluidics with different flow strength.



Figure 4.1 Image shows the Opto-Fluidic chip for cell viability tests. Diameter of well is 5 mm. Height is 2 mm. Fully fill each well and add cover slip on top to get a clear vision when observe it using microscope.

The motivation of this research is to develop a testing device that can rapidly detect pathogenic bacteria and any cellular constituents which are critical for diagnosis from liquid bio-samples. Therefore, a biocompatibility testing on bacteria and human cells are necessary for the prototype of device, which is Opto-Fluidic chip. One species of bacteria named *Bacillus. subtilis* is chosen as representative of prokaryotic cell. The human lung fibroblast cells are chosen as representatives of eukaryotic cells. Both type of cells is commonly used in biological & medical experiments. Therefore, we use them to test the biocompatibility of Opto-Fluidic chip.

Bacteria can grow in bacterial culture medium. To prepare the bacteria sample for test, we use sterilized PBS solution to dilute the bacterial culture medium, for getting an appropriate concentration of cells. In final samples, the concentration of bacterial cells remains around 10^3 - 10^5 per microliter. This range of concentration can give us a clear microscope view. We can observe the distribution of cells under the influence of Opto-Fluidics. Similarly, to prepare the fibroblast cells suspension, we first culture the lung fibroblast cells in petri-dish and let cells

reproduce inside. Fibroblast cells can grow and proliferate when they adhere to surface of petri-dish. Then we use enzyme to treat adherent cells, let cells detach from surface of petri-dish. Then we add sterilized PBS solution to wash and suspend cells. The concentration of fibroblast cell suspension is set around $10 - 10^3$ per microliter.

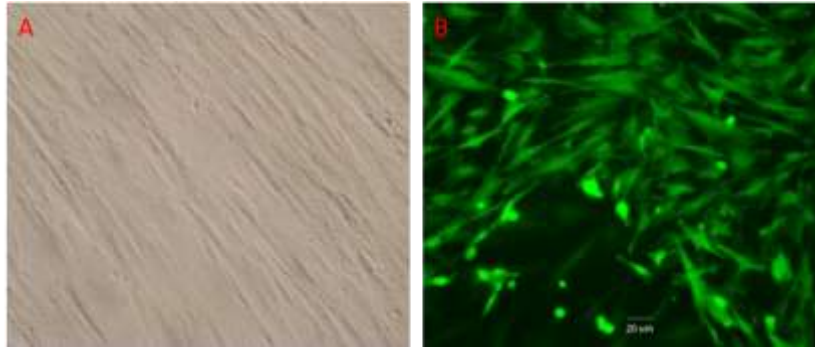


Figure 4.2 Images show the normal cellular morphology of fibroblast cells in bright-field and fluorescence field. Image A shows normal cells look under bright field; B is fluorescence image of cells. Cells are robust and can emit strong green fluorescence after being stained by Live/Dead Cell Imaging Kit. The 20-um scale bar locates at the middle bottom of image B.

After both type of samples are prepared, we test the fibroblast cells at first. We add fibroblast cells suspension into a reservoir on chip. Then we turn on laser to generate Opto-Fluidics inside the reservoir. The fibroblast cells are manipulated in low power (5 mW, Figure 4.3a), medium power (40 mW, Figure 4.3b), and the high power (80 mW, Figure 4.3c). Base on images (Figure 4.3a2, b2, c2), we can clearly tell that cells aggregate much severely along with increase in power. The cells in each well are manipulated for 300 seconds, after which, the whole chip is sent into an incubator, where the cells are cultured for 24 hours. During the period of incubation, the cells adhere to the gold surface and start growing. Bright-field microscopy demonstrate that the cells look healthy and have an expected morphology (Figure 4.3a3, b3, c3). We then use a live/dead cell imaging kit to stain live cells with green-fluorescence-emitting dye, and dead ones with red-emitting dye. It is confirmed using fluorescence imaging that the cells appear healthy and emit a green fluorescence signal (Figure 4.3a4, b4, c4). After a detailed examination, on average, less

than one dead cell is observed per well, matching the results from the control well that was not exposed to any manipulations. This result confirms that opto-fluidic manipulation under different power levels is biocompatible and does not decrease cell viability. Meanwhile, we compare the cell morphology of Figure 4.3 with the standard cell morphology from Figure 4.2 and conclude that the Opto-Fluidic treatment on cell does not change the cellular morphology.

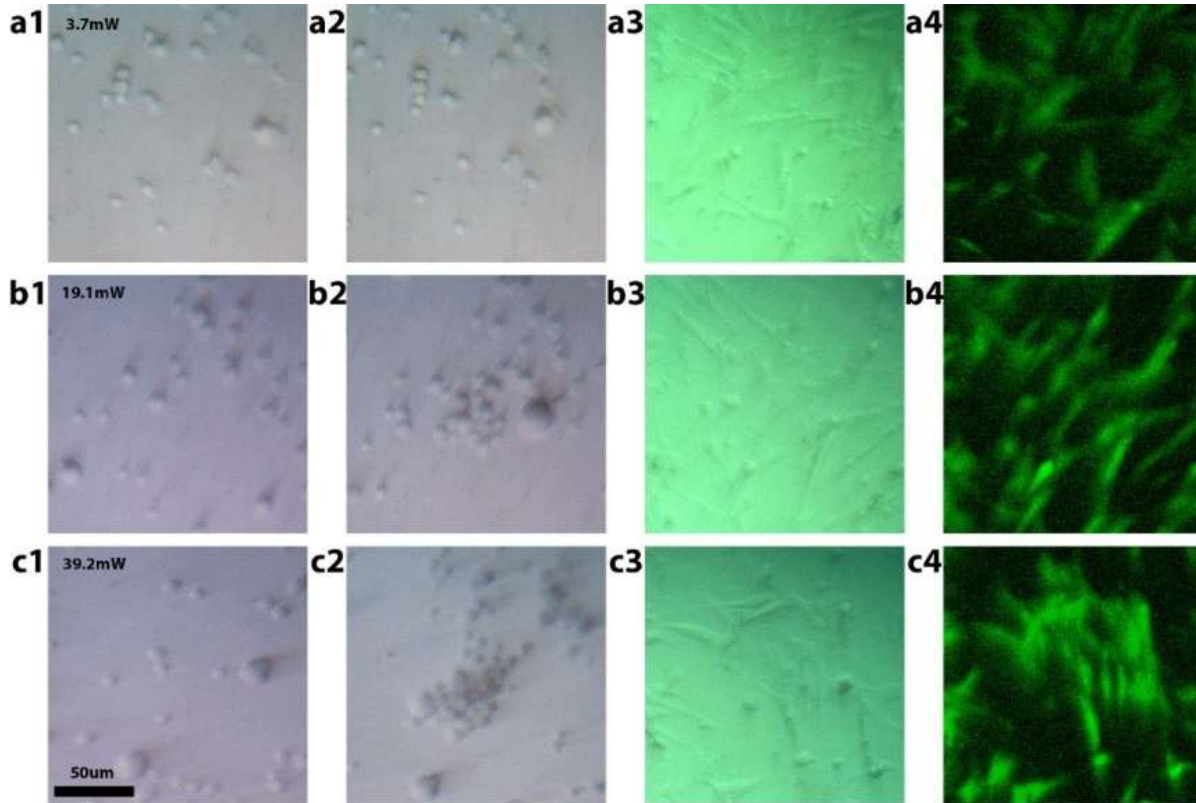


Figure 4.3 Demonstration of fibroblast cell viability after opto-fluidic manipulation. Before and after low-power manipulation at 5 mW (a1, a2). Before and after medium-power trapping at 40 mW (b1, b2). Before and after high-power projection regime at 80 mW (c1, c2). Bright-field (a3, b3, c3) and fluorescent images (a4, b4, c4) of cells after 24 hours of incubation.

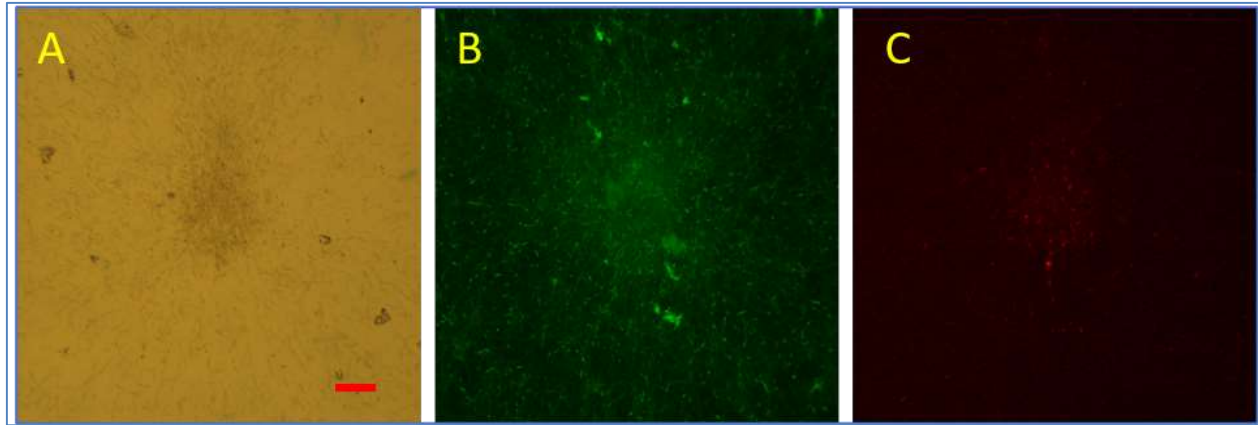


Figure 4.4 Images demonstrate that the majority cells in the bacteria aggregation are alive. Image A is taken under bright field. Dark spot in middle shows the aggregation. Image B is fluorescence image only shows green fluorescence signal from sample. Image C only shows red fluorescence. A 10X magnification lens is used. Exposure time is 1 millisecond for bright field and 1second for the fluorescence field. Laser power is 20 milliwatt. Scale bar is 100 ums.

Subsequently, we use bacteria sample to test the biocompatibility of chip as well. Bacteria are stained by Live/ Dead Bacterial Viability Kit in advance. This staining kit can be used to assess the viability of bacterial populations. The staining of cells depends on the membrane integrity of cell. Cell with compromised structure of membrane that are considered to be dead or dying will be stained in red. Meanwhile, cells with intact membrane will be stained in green. After staining, the bacteria suspension is added into the reservoir on chip. Then, we set the laser power at 20 mW, which is very effective for concentrating bacterial cells. The Figure 4.4 shows bacteria aggregation appears after being treated with OFM for 20 minutes and can be viewed under both bright field (image a) and fluorescence field (image b & c). Compare image b and c, we can conclude that the area of green fluorescence is larger than the area of red, and intensity of green is much stronger than red. This result proves that most *B. subtilis* bacteria cells can remain alive after been concentrated on Opto-Fluidic chip for 20 minutes. The power of laser can vary from 5 mW, to 40 mW. Cell viability under higher laser power (>40mW) is unknown from this experiment. The

reason we did not give it test because there will be no more bacteria aggregation under higher power of laser.

4.2 Conclusion

The Opto-Fluidic chip which has multiple wells structure is used for doing biocompatibility test. Both bacterial cells and human cells are tested on the chip. This test results can be equivalently used on another Opto-Fluidic chip which has microfluidic channel structure. We use the Live / Dead viability kit to stain cells at the beginning of experiment, to better identify the status of cells. In bacteria tests, the dye can even be a real time indicator of cell status. Because the plasma membrane of bacteria cells will be ruptured if the test lead to cell necrosis [61]. The dead cells with compromised structure of membrane will be stained in red. Meanwhile, alive cells will be stained in green. As a conclusion, we clearly see both human lung fibroblast cells and the majority of *B. subtilis* cells are alive after been tested on chip. These experiment results can demonstrate that the Opto-Fluidic chip is highly unlikely can cause damage or death on cells. For fibroblast cells, the safe laser power range is 0 ~ 80 mW. For *B. subtilis* cells, the safe laser power range is 0 ~ 40 mW. Effect by the laser power beyond this range is unidentified.

³Chapter 5: Bacteria Separation Using Opto-Fluidic System

In the previous chapters, we develop the Opto-Fluidic chip with optimized structure. Then, we build up a system that enable the Opto-Fluidic chip to process both static liquid sample and flowing samples. The Opto-Fluidic chip can concentrate, and isolate small particles from sample. Besides, the biocompatibility tests on the chip demonstrate that cells such as *B.subtilis* bacteria and human lung fibroblast cells can endure the manipulation by Opto-Fluidics while not lose their viability. Therefore, we decide to use the Opto-Fluidic manipulation system to isolate a certain type of cells out from bio-samples. For instance, we can try to isolate bacteria from either urine or blood. Both operations have critical clinical significance.

Sepsis as a typical blood infection complication, is a potentially lethal condition usually caused by enhanced immune response to an infection. It currently affects more than 1 million Americans per year with 15-30% mortality rate [42]. The number of sepsis cases per year has been on the rise in the United States, and rapid rise of antibiotic resistance poses a significant problem in how we treat these cases [43]. Bacteria, such as *Escherichia coli*, *Streptococcus pneumoniae*, and *Staphylococcus aureus*, are the most commonly encountered microorganisms in sepsis patients [44]. Antibiotics are prescribed to treat infections caused by bacteria including bacterial sepsis [45]. Generally, 2 days are required for the positive identification of the bacterial species causing infection and for the testing of candidate antibiotics to determine the most effective treatment

³This chapter was published in Biomedical Optics Express...Reference [21](Wang, Hao, et al. "Innovative optofluidics and microscopy-based rapid analysis of pathogens." Biomedical Optics Express 11.9 (2020): 5060-5069.). Permission is included in Appendix: Copyright Permissions

option. Unfortunately, time is often limited, and as a result, antibiotics are prescribed empirically without proper testing. Consequently, treatments can often be inefficient, and the unneeded exposure of bacteria to antibiotics paves the way for rise in antimicrobial resistance. Additionally, reports show that many patients with sepsis exhibit negative blood culture results even after several days [46], indicating that it is possible to not detect some microorganisms using conventional approaches.

Similar time-related constraints are problematic in the testing of other biological fluids. For example, the laboratory examination of urine specimens accounts for a large part of the workload in hospital laboratories. Unfortunately, traditional approaches for processing urine cultures, and subsequent antimicrobial testing, requires 2 to 3 days [47]. This significantly delays treatment and negatively affects the outcome of the patient, if the empiric antibiotic prescription was suboptimal. As a result, there is an urgent need for new technologies that allow for prompt detection of bacteria in biological samples, followed by rapid antibiotic selection, to decrease the time it takes to inform and guide the prescribing physician.

Currently there are several alternative approaches focused on speeding up the identification of optimal antibiotics for treating infections. For example, PCR-based assays, such as multiplex-PCR, can deliver results differentiating between bacteremia vs fungemia in approximately 6 hours [48]. However, this requires additional steps to precisely identify the disease-causing agent and to perform the antibiotic susceptibility testing [49]. Another approach is to use mass spectrometry combined with the database of the peptide mass fingerprints of known pathogens to identify microorganisms [50]. Peptide nucleic acid (PNA) fluorescent in situ hybridization (FISH) stains (AdvanDx) are commercially available for direct identification of selected pathogens from positive blood cultures [51]. Electrochemical sensor assays can be applied to rapid (30 min) genotypic

identification of bacterial pathogens [51]. Additionally, the Verigene gram-positive blood culture test can be used for identification of 12 gram-positive bacteria and 3 genetic markers of antibiotic resistance directly from positive blood culture medium [51]. Flow cytometry can be also applied to bacterial identification [52]. Unfortunately, the main drawback is that these techniques require culturing bacteria, and only can be conducted after significant time delays [51]. Additional time delay is introduced because of the antibiotic susceptibility testing.

An alternative approach is to use signature molecules, such as pathogen-associated molecular patterns (PAMPs) that are specifically present in bacteria and fungi and can be used to quickly identify the nature of the disease-causing agent. In fact, a recent study using enzyme-linked lectin-sorbent assay (ELLeSA) has showed promising results using this technique in identifying pathogens [53]. Other approaches include single molecule scanning (SM-Scanning) [54,55], or electrochemical-based detection that depends on the presence of 16S rRNA of bacteria [56]. In line with the other methods that are being developed to address this major problem in pathogen analysis, we propose a new approach to analyze biological fluids using an optofluidic technology developed by our laboratory [37] for rapid concentration of bacteria followed by rapid antibiotic screening. There are several other methods focused on the use of microfluidics for isolation of bacteria from blood [57,58]. One of them was focused on isolation and concentration of bacteria from blood using microfluidic membraneless dialysis and dielectrophoresis. This approach is very different from proposed here since it is based on electrical properties of all components, and also requires change of the conductivity of the fluid to operate. Another interesting approach to bacterial isolation is based on elasto-inertial microfluidics. It achieves good isolation performance and works reliably with whole blood, but currently can only process 60 $\mu\text{L}/\text{hour}$, even though some parallelization designs were proposed [58].

As far as concerned, the timely knowledge and prescription of the most suitable antibiotic to treat bacterial infections is critical for the recovery of patients battling life-threatening bacterial infections. Unfortunately, current standard-of-care approaches relies on the empiric prescription of an antibiotic, as determination of the most effective antibiotic requires multiple time-consuming steps. These steps often include culturing of the bacterium responsible for infection and subsequent antibiotic susceptibility testing. Therefore, we want to know if the Opto-Fluidic system allow us to capture bacterial cells from blood samples and use the captured bacteria for rapid antibiotic selection thereby bypassing the need to culture the bacterium.

5.1 Methods

The first step required for antibiotic selection testing is isolation of bacteria from a biological sample. There are two challenges that we face while isolating bacteria from the samples. First, bacteria might be present in low concentrations and thus must be preconcentrated. Second, there are many other particles and cells present in those samples. This makes traditional techniques based on micro-scale filtering challenging, since it is much easier to isolate larger objects (e.g. circulating tumor cells or blood cells), than tiny bacteria present in low concentration. Because of that we are proposing to use optofluidic particle manipulation that allows us to selectively concentrate micro-scale objects of a desired size that we previously demonstrated on a variety of micro-particles and cells.

Figure 5.1 shows the schematics explaining the mechanism of optofluidic concentration of bacteria. One of the critical components of the system is a specially designed bi-metallic substrate. It consists of a glass slide with sputtered layers of chromium and gold optimized for efficient absorption of green light and local fluid heating. In the prior publication we conducted detailed simulations and experimental optimization of the substrate and demonstrated that it works most

efficiently when we use glass slides with sputtered 5 nm of chromium and 200 nm of gold. The wavelength of the laser used in all manipulations is 532 nm. All fluorescence microscopy is conducted from the top side of the substrate, while laser heating is done from under the substrate. This way sample is not exposed to the laser light and quality of the fluorescence imaging is not compromised.

Figure 5.1(a) shows a drop of fluid sample under a microscope objective on a bi-metal substrate. A cleaved tip of an optical fiber is placed under the substrate. Light is coupled into this fiber from a laser with a wavelength of 532 nm and an adjustable power. Light from the fiber tip locally illuminates the substrate, gets partially absorbed by the bi-metallic layer and locally heats the fluid. Warm fluid rises to the top, and this results in the generation of a toroidal convection current (Figure 5.1(b)). The horizontal part of the current, shown with yellow arrows, can be used to trap micro-scale particles, while the vertical section, shown in red, can be used to levitate them. This setup can be used to capture, sort, and separate particles based on their size [14]. For example, for the fluids containing a mix of particles of two significantly different sizes, we can independently control each particle population. With a low laser power, we can capture small particles without moving large ones. Alternatively, with higher laser power we can capture both large and small particles, but then remove and separate small ones by levitation, while keeping large ones on the surface of the substrate [14]. Therefore, particles can be controllably separated based on size. For our specific application we concentrate bacteria without moving other cells present in the sample and without phototoxicity or significant heating.

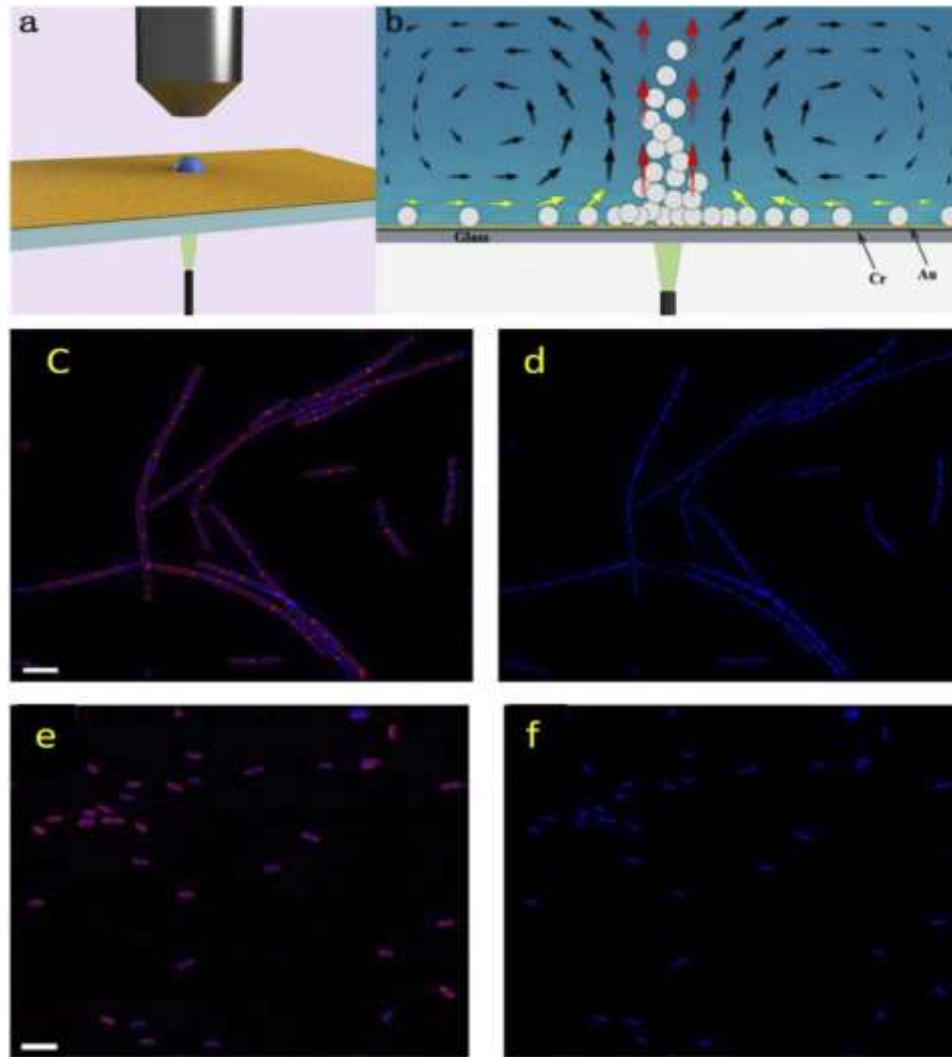


Figure 5.1 Experimental setup and bacteria used for manipulation. a) A 3D model of the experimental set up for optofluidic manipulation of bacteria. The bi-metallic substrate is horizontally placed in between the microscope objective and an optical fiber with a metallic layer facing up. The lens and the optical fiber are aligned, so the spot on the substrate exposed to the light from the fiber is imaged using the objective. The liquid sample is dropped on the substrate, and then light is turned on. B) shows a zoomed-in cross-section of the droplet on the substrate after light is turned on. The symmetric vortex is formed, and bacteria shown as white circles are concentrated around the heated spot. Image c) and d) show *B. subtilis* wild type strain PY79. Image e) and f) show *E. coli* wild type strain K12. Both species have their cell membrane stained red with FM4-64, which can be observed in c) and e). Blue fluorescence indicates the location of DNA inside cells via DAPI stain. Scale bar is 5 μm .

In these experiments we used two types of bacteria (gram-positive and gram-negative) with very different cell characteristics to demonstrate that our approach works equally well for different bacterial species (Figure 5.1(c-f)). Wild type *Bacillus subtilis* (PY79), which is a gram-positive

model organism, often forms chains of cells during exponential growth (Figure 5.1(c) and (d)). Wild type *E. coli* (K12) is a gram-negative model organism (Figure 5.1(e) and (f)). Bacterial cells were stained by 4',6-diamidino-2-phenylindole (DAPI) in order to visualize DNA. When bound to double-stranded DNA, DAPI has an absorption maximum at a wavelength of 358 nm (ultraviolet) and its emission maximum is at 461 nm (blue). Also, the cell membranes of the bacterial cells were stained with FM4-64 fluorescent dye (excitation/emission maxima 515/640 nm), emitting red fluorescence signal.

5.2 Experiment Results

5.2.1 Concentration of Bacteria

We have previously demonstrated that we can concentrate particles and cells in water and buffer [14], however real biological samples are much more complex, and have a variety of particles and cells of different sizes. The goal of the following experiments was to demonstrate that size-dependent isolation of bacteria can be conducted in real biological samples. The experimental condition should be altered depending on the bacterial load in samples.

Figure 5.2 shows a diluted rat blood sample spiked with bacteria. Whole blood was diluted with standard phosphate buffer saline (PBS) 2000 fold, and then mixed with *B. subtilis* cells (CFU approximately equal to 2×10^7 per ml) the volume ratio of 1:1. The final sample volume was 50 μ l and the laser power was 25 mW. Image a) and d) are the 3D rendering made using Autodesk Inventor created for easier understanding of the difference between the experiments. Parts b, e shows bright field microscopy images with dark dots representing individual red blood cells, while both Figure 5.2(c) and (f) are fluorescence images taken in the same field of view but showing DAPI-stained bacteria.

At first, both bacteria and red blood cells are evenly distributed on the substrate. After 2 min of optofluidic concentration, bacteria aggregated in one spot. Figure 5.2(b) shows cell distribution before optofluidic manipulation and e) after manipulation, while bacteria are difficult to see because of the small size and transparency. Figure 5.2(c) and (f) are fluorescence microscopy images taken under UV excitation. Since *B. subtilis* cells are stained by DAPI, the cells emit blue fluorescence with a peak at 461 nm. Image c) shows that bacteria are initially distributed evenly. After two minutes of optofluidic manipulation bacteria aggregate above the optical fiber (Figure 5.2(f)). This way we can independently track populations of the RBCs and bacteria and demonstrate local concentration of bacteria in a blue spot (Figure 5.2(f)) with much darker area around the spot.

The left part of the Figure 5.2 demonstrates that relatively high concentrations of bacteria can be manipulated using optofluidics, and the right part shows a similar experiment conducted at much lower concentration of bacteria. The bacterial sample was diluted 2000-fold (100X less concentrated than in the left images). The diluted bacteria sample was mixed with diluted whole blood at a volume ratio of 1:1. Since the initial number of bacterial cells is low (CFU reaches as low as 5×10^3 per ml), initially there are no bacteria in the field of view of the microscope, and only after the optofluidic concentration we are able to see several bacterial cells. This demonstrates that optofluidic concentration of bacteria works for a wide range of concentrations of cells.

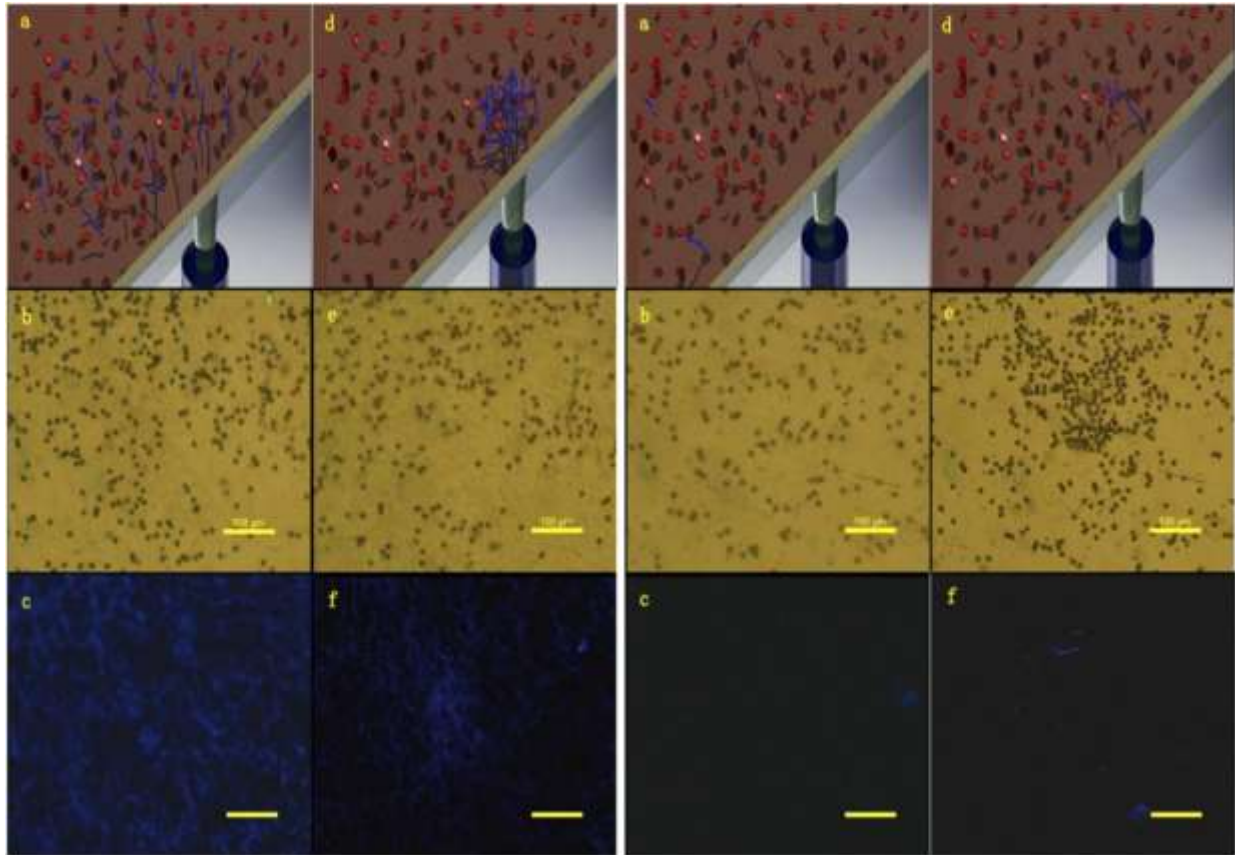


Figure 5.2 Two sets of images demonstrate that both high (left set) and low (right set) concentrations of bacteria can be aggregated after 2 minutes of optofluidic manipulation. Images a) - c) show the original distribution of cells and d) - f) show cell distribution and bacteria aggregate after optofluidic manipulation. a) and d) are artistic renderings, b) and e) bright field images, and c) and f) fluorescence images. Laser power was 25 mW in both tests. Scale bar on each image is 100 μm .

The next experiment demonstrates that the optofluidic bacterial concentration works equally well for bacteria with very different cell characteristics and for a different type of biological specimen. Here a sample was prepared by mixing fibroblast cell suspension with *E. coli* in the volume ratio of 100:1. At first, we cultured human lung fibroblast cell (IMR-90) in a petri-dish. Fibroblast cells, unlike blood cells, are anchorage-dependent cells which can only grow when attached to a substrate. To harvest the cells, a standard protocol for cell detachment was used. As soon as we obtained fibroblast cells suspension, it was immediately mixed with the bacterial suspension (CFU approximately equal to 1×10^9 per ml). The sample volume was again 50 μl , and

the laser power was 30 mW. Figure 5.3(a) is a bright field image after optofluidic concentration of bacteria, while Figure 5.3(b) is a fluorescence image. The blue spot in the Fig. 25(b) is a cloud of concentrated bacteria. Interestingly, in Figure 5.3(a) we observed a dark spot in the bright field image. This indicated that, at least for *E. coli* the concentrated bacteria can be observed in the bright field. Figure 5.3(c-e) shows that the cloud of bacteria accumulates over time. Initially it is absent (Figure 5.3(c)), then it starts forming after one minute of optofluidic manipulation (Figure 5.3(d)). Finally, many bacterial cells are captured after one more minute (Figure 5.3(e)). Figure 5.3(b) shows that the area around the bacteria cloud is free of other cells, demonstrating that most of the bacteria from the sample is now concentrated in a single spot.

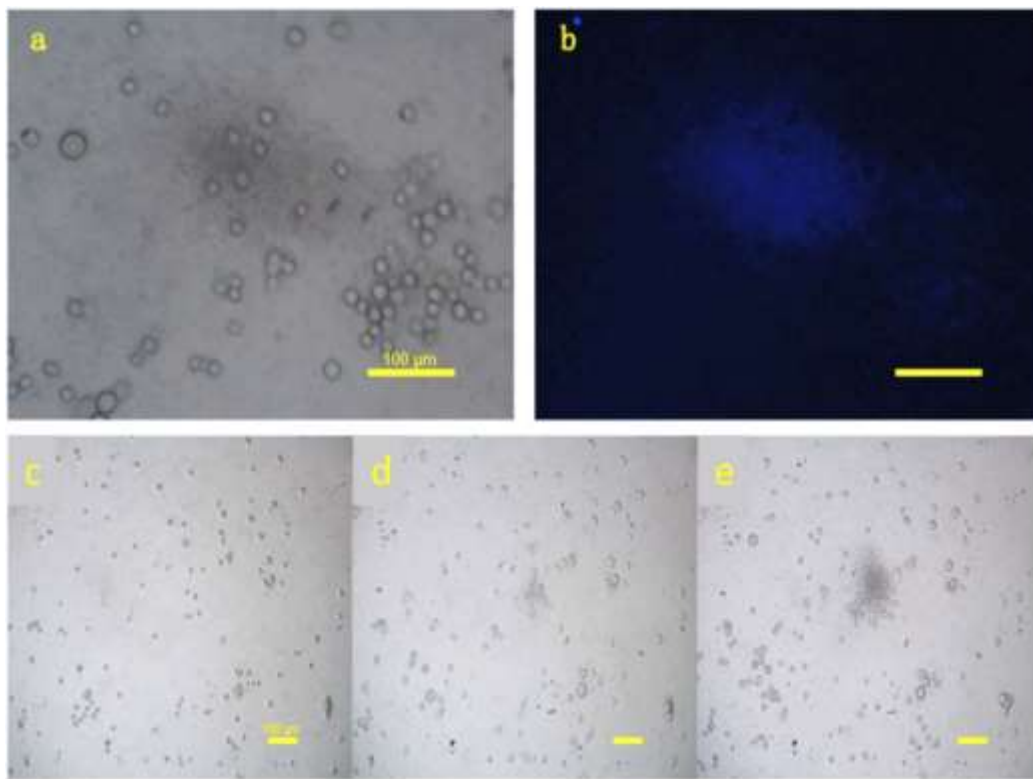


Figure 5.3 Optofluidic concentration of *E. coli*. *E. coli* cells were stained with DAPI emitting blue fluorescence light under UV illumination. a) The round transparent objects are fibroblast cells, they do not move under optofluidic manipulation. b) The blue cloud is a fluorescence image of the bacteria concentrated in a single spot. c)-e) show gradual formation of the bacterial cloud. Scale bar is 100 μm.

5.2.2 Isolation of Bacteria

Concentrated bacteria have to be isolated from the sample and used for antibiotic screening. It can be done by integrating the optofluidic manipulator on a microfluidic chip. Figure 5.4(a) shows the microfluidic setup used for capturing of the concentrated bacteria with a thin needle. The sample is injected into a microfluidic channel through the inlet, the bacteria are concentrated, and removed using a thin sharp needle which was prefabricated inside of the channel. The optofluidic bacteria concentration step isolation step is conducted in front of the needle tip. After that, the small amount of fluid with the concentrated bacteria can be pumped through the needle outside of the microfluidic channel for further antibiotic screening. Subsequently, the fluid sample with removed bacteria is pumped out through the second outlet, and “concentrate-isolate-pump” steps can be continuously repeated to process larger sample volume. In the future we plan to integrate isolation chip with the screening chip into one continuously operating microfluidic system.

In the experiment in Figure 5.4(b-I), DAPI-stained *B. subtilis* cells were injected in a microfluidic channel, and the bacterial cloud was captured after 10 min of optofluidic concentration. It can be noticed as a flow of dark/blue material in a direction of the needle tip (Figure 5.4(f,g)). The captured bacteria were released on a different substrate and were concentrated again (Figure 5.4(h-i) and Figure 5.5). Fluorescence emitted by the bacteria can be used to determine transfer efficiency. We use the Photoshop Histogram tool to extract the integrated blue color intensity of the section inside yellow circle in both images. It was demonstrated that ~60% bacteria could be successfully captured, transported to a different substrate and re-concentrated.

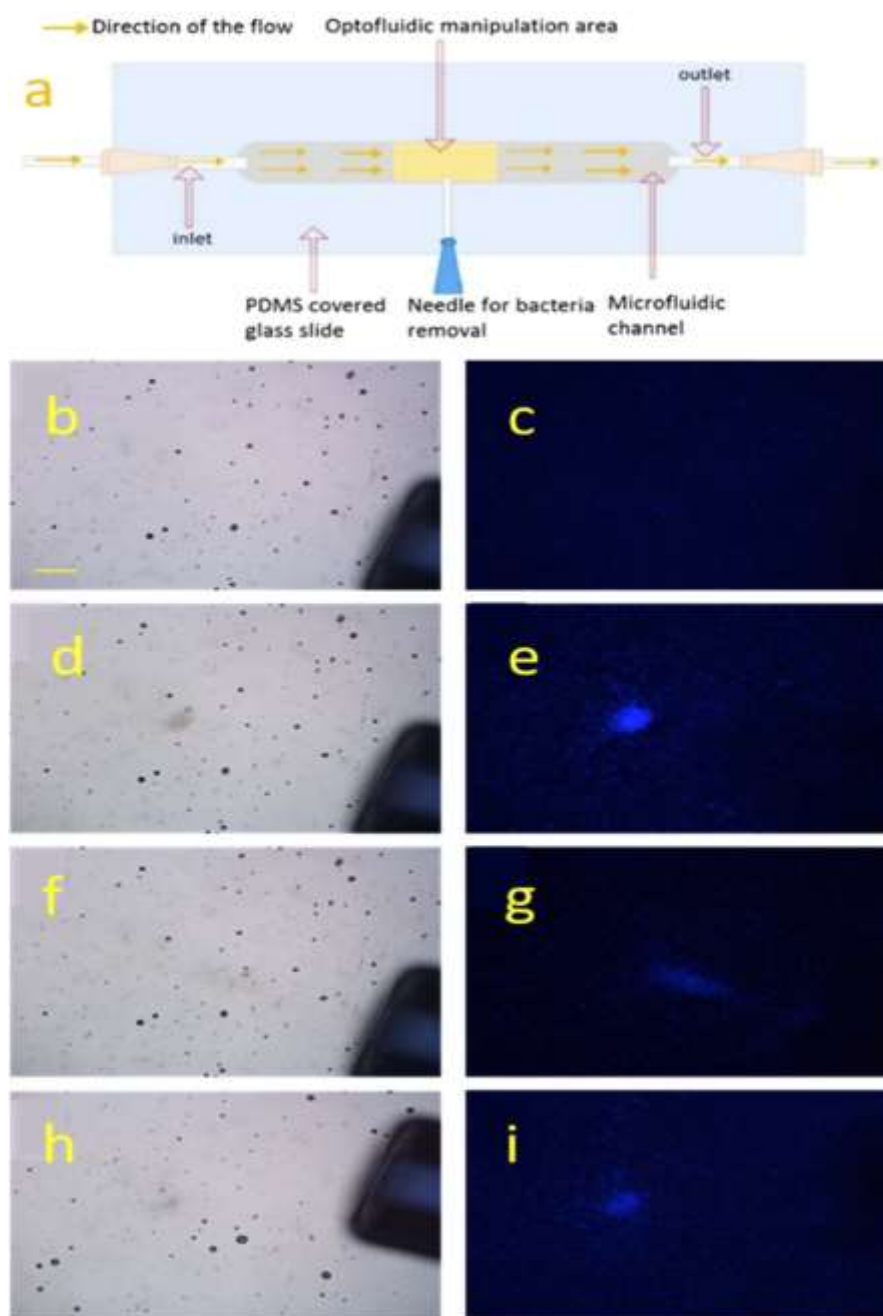


Figure 5.4 Schematics of an experimental setup with a microfluidic channel for capturing of concentrated bacteria for further analysis followed by experimental results with DAPI-stained *B. subtilis*. The bright field and fluorescence images were obtained over the same field of view to demonstrate the position of the needle and the bacteria. The optofluidic concentration was conducted for 10 min using 25 mW laser power, and bacteria were captured in one bright spot. Then the bacteria cluster was removed through a syringe needle connected to a microfluidic pump through tube (flow rate was $<10 \mu\text{l}/\text{min}$). The bacteria cluster in $50 \mu\text{l}$ of solution was released onto a new chip for further analysis. The scale bar is $100 \mu\text{m}$.

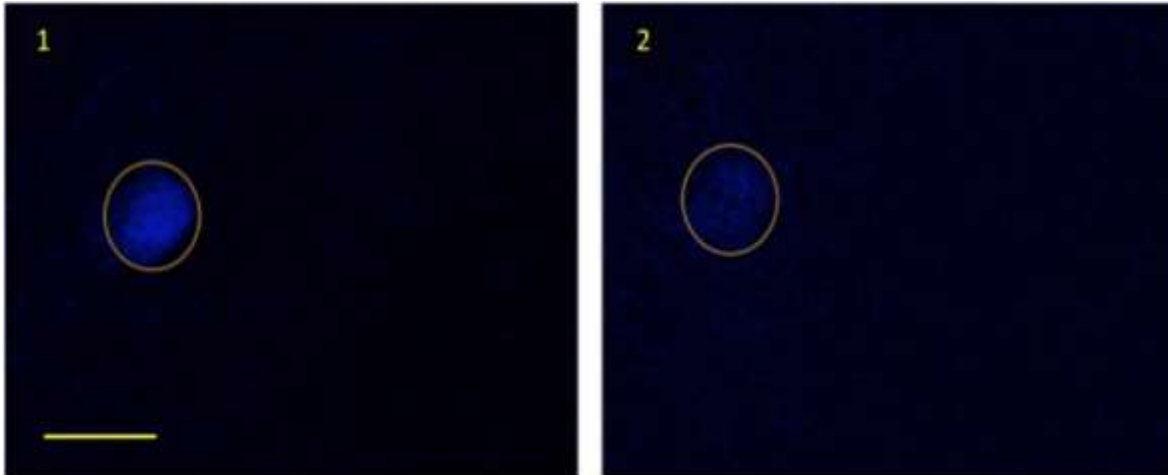


Figure 5.5 Magnified view of the initial concentrated cluster of bacteria (1) and one obtained after re-concentration (2). Both images were taken under identical imaging conditions, and at least 60% of bacteria was successfully captured, transferred and re-concentrated. Laser power was 25 mW. The scale bar is 100 μm .

5.2.3 Rapid Antibiotic Screening

In order to test our ability to perform rapid antibiotic screening for different types of bacteria, we imaged wild type and ampicillin resistant (AmpR) *E. coli* (a gram-negative bacterium) and *S. aureus* (a gram-positive bacterium). The cells of these strains were treated with ampicillin, a bactericidal antibiotic that inhibits peptidoglycan synthesis and causes cell lysis. As shown in Figure 5.6, while the wild type cells were susceptible to ampicillin (as indicated by cell lysis), as expected, ampicillin-resistant *E. coli* and *S. aureus* cells did not show any lysis upon ampicillin treatment. The concentration of ampicillin (8 $\mu\text{g/ml}$) selected closely follows the clinically relevant minimum inhibitory concentration.

In practical use, after the concentrated bacteria were isolated from sample by using the microfluidic chip and thin needle, the concentrated bacteria sample was equally divided into several aliquots. Different aliquot was respectively mixed with different antibiotics. Then we use optical microscopy to figure out which type of antibiotics can most efficiently cause cell lysis.

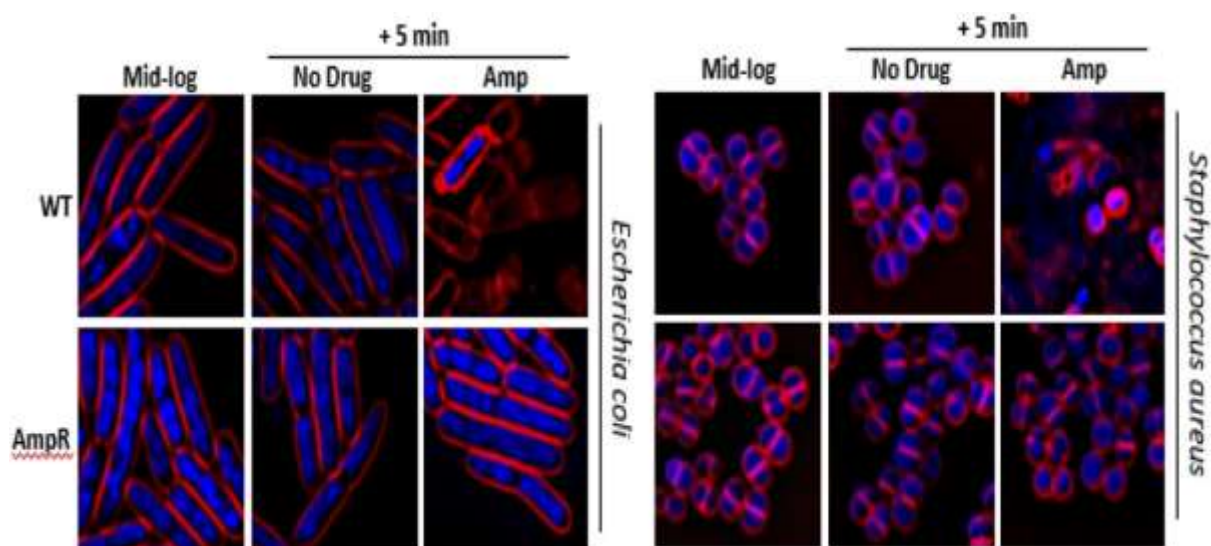


Figure 5.6 Fluorescence microscopy was used to determine the susceptibility of wild type (WT) and ampicillin-resistant (ampR) *E. coli* cells as well as WT and ampR *S. aureus* cells to the treatment of ampicillin. Cells were grown to mid-logarithmic phase and an aliquot of sample was imaged. Next, cells were treated with 8 $\mu\text{g/ml}$ ampicillin for a period of 5 min and subsequently imaged to determine susceptibility to the drug. Untreated cells grown for the same duration of time at the same temperature were used for comparison. Cells were stained with DAPI (DNA; blue) and FM4-64 (membrane; red) and imaged at mid-log phase growth (no drug), 5 min later (no drug), and 5 min later (drug). Ampicillin-sensitive strains lysed in the presence of the drug, whereas ampicillin-resistant cells were able to survive ampicillin treatment. This demonstrates that real-time testing of bacteria with antibiotics can be easily monitored under the microscope.

5.3 Conclusion

We have demonstrated that different types of bacteria in various biological samples can be efficiently concentrated and isolated for further testing. The concentration approach works for diluted blood and cell growth media. Presence of cells does not prevent efficient concentration of bacteria. This approach works well for bacteria with very different cell structure, and for a wide range of concentrations from under 2.5×10^2 cells in a 50 μl sample to 100X more concentrated. The concentrated bacteria can be isolated from the sample using a microfluidic chip and a thin needle, transferred to a different substrate and re-concentrated with at least 60% efficiency. The live bacterial sample can be analyzed using rapid antibiotic screening using microscopy to observe morphological changes produced by the administration of an antibiotic. Significant difference was

observed after administration of the drug to the wild type and the drug-resistant strains. The testing is done optically on a small number of live bacteria and the susceptibility to different antibiotics can be visualized within minutes from the beginning of the assay. Once bacterial cells are isolated from the biological sample, the effectiveness of bactericidal antibiotics can be determined in approximately 1 hour. This is significantly less time than the standard 24-48-hour cultures that are generally required using a conventional approach. Overall, this technology can greatly speed up the identification of appropriate antibiotic in case of bacterial infections

Chapter 6: Opto-Fluidics Induced Antibody Immobilization-Based Rapid Detection

The first simulation of Opto-Fluidics in chapter 2 shows the 2D cross-section of the temperature distribution in a circular well and the streamline plot of fluid forms symmetric loops (Figure 2.2). In the experiment, the Opto-Fluidics will have toroid shape convective flows inside the circular well. Microbeads located on the bottom surface of well can move towards the bottom center of the toroid and aggregate there (Figure 2.3). This phenomenon has been shown in many experiments previously. The Opto-Fluidics are strong enough to move microparticles that settled on surface of substrate. Therefore, we want to know if these convective flows can be used for different purposes other than microparticle concentrating.

Coincidentally, we find two research that both use high intensity sound wave to induce fluid motion on solid surface. This type of fluid can be called micro-mixing or micro-agitation. The antigen-antibody specific binding is commonly used for detecting protein molecules. Either molecule from antibody-antigen pair can be immobilized on solid surface as probe molecules, to detect its paired molecule from sample. Base on experiments from one research, the fluid motion on surface can be used for removing the non-specific molecule bindings. Additionally, the fluid motion can also decrease the antibody-antigen incubation time [60].

Another application of acoustic streaming on surface is presented by the second research. It is used in DNA microarray for enhancing the results. The core principle of microarrays is hybridization of molecules. It is the process of combining two complementary single-stranded DNA or RNA molecules and allowing them to form a single double-stranded molecule through

base pairing. Same as protein molecule detection chip, a collection of microscopic DNA spots attached to a solid surface. There can be several thousand spots on one microarray chip. The sample loaded on chip requires incubation to complete the molecule hybridizations [59]. A very small sample volume can be physically agitated by using surface acoustic wave. This micro-mixing or agitation inside liquid sample can lead to the reduction of incubation time for hybridization and increasing of signal-to-noise ratio [59]. Based on two research, we can conclude that the fluid motion on surface can increase the motion rate of molecules in sample, subsequently lead to a higher chance of encounter its complementary probes which are fixed on surface.

Meanwhile, the Opto-Fluidics we generate on substrate contain microfluid motions as well. These fluid motions stem from convection can also be regarded as micro-agitation or micro-mixing. Theoretically, the Opto-Fluidics can cause a similar effect as the acoustic streaming did to microarray chip. To verify this idea, we need to let either antibody-antigen specific binding or the nucleic acid hybridization takes place on thermal-plasmonic substrate. To make this happen, the substrate requires a special surface treatment. The goal of surface treatment is immobilizing molecular probes on gold surface. In our case, we only choose to test the antibody-antigen specific binding on substrate, as the first tentative trial.

To visualize results of molecules binding on surface, we should use fluorophore conjugated molecules. Molecules that bind to probes can stay on surface after flush. Therefore, the total number of captured molecules on surface can be visually quantified by measuring the fluorescence intensity. Through contrast tests, we will identify whether Opto-Fluidics can facilitate the specific binding of molecules on surface.

6.1 Methods and Experiment Results

The first step of experiment is that we need to immobilize the molecular probes tightly on the thermal-plasmonic substrate. Meanwhile, a sample container which is built on top of substrate is necessary for the generation of Opto-Fluidics. Regarding the candidate of molecules pair used in experiments, we choose the bovine IgG as molecular probe which will be immobilized on substrate, and fluorophore conjugated anti-bovine IgG as molecules being tested. The fluorescent antibody solution as sample will be added onto substrate in experiments.

Before we immobilize molecules on substrate, we are aware of one fact that is the surface of substrate is not free of contaminations. The contaminants on gold surface can prohibit the immobilization of molecular probes. Therefore, a thoroughly cleaning of gold surface is critical for the following steps. An appropriate cleaning protocol is applied on substrate for removing all contaminants from the surface of gold. Meanwhile, try to maintain molecular-level cleanliness of surface as much as we can during entire experiment.

Next, the gold surface requires special treatment with chemicals to make protein molecules binding on it, because normally protein molecule cannot form strong bond with gold. We intentionally apply two methods respectively which both are widely used for immobilizing protein on gold. We want to identify which method can give a better performance on substrate. Each method will introduce a linker molecule on surface. The linker molecule is an inorganic long-chain molecules, and it can form strong bonds with gold. One end of linker molecule binds on gold while another end can form covalent bonds with protein molecule. Gold surface treated by method A has APTES [(3-Aminopropyl)triethoxysilane] as linkers. Meanwhile, surface treated by method B has DSP [dithiobis(succinimidyl propionate)] as linkers. Next, we add the fluorophore labeled antibody solution on two different treated substrates. Let the solution incubate on substrate for the

same amount of time. At last, gently wash surface with water and put the treated surface under microscope for the fluorescent signal check.

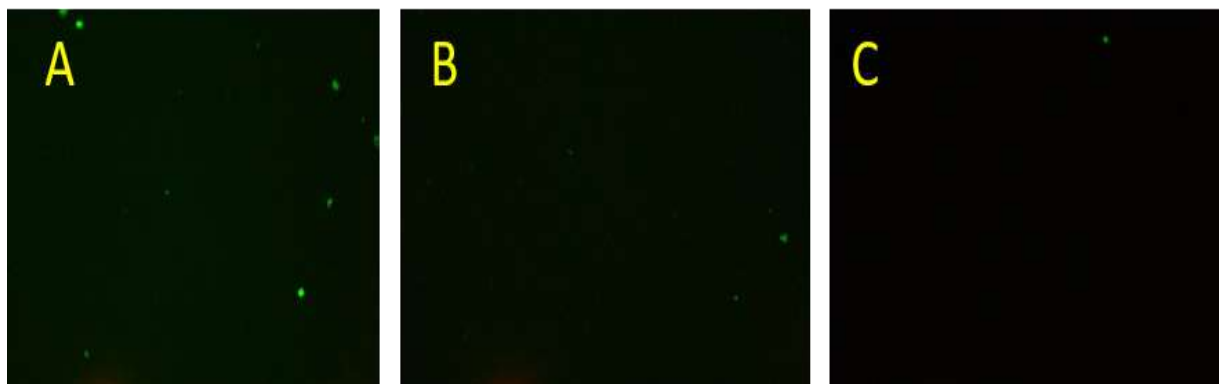


Figure 6.1 Images show fluorescence on gold surface of three samples. Image A shows surface has DSP as linkers, fluorescent IgG solution (50ng/ml) stays on surface for 24 hours then flush surface. Image B has DSP as linkers, fluorescent IgG solution (5ng/ml) stays on surface for 24 hours then flush surface. Image 3 shows surface has no linker, fluorescent IgG solution (5ng/ml) stays on surface for 24 hours

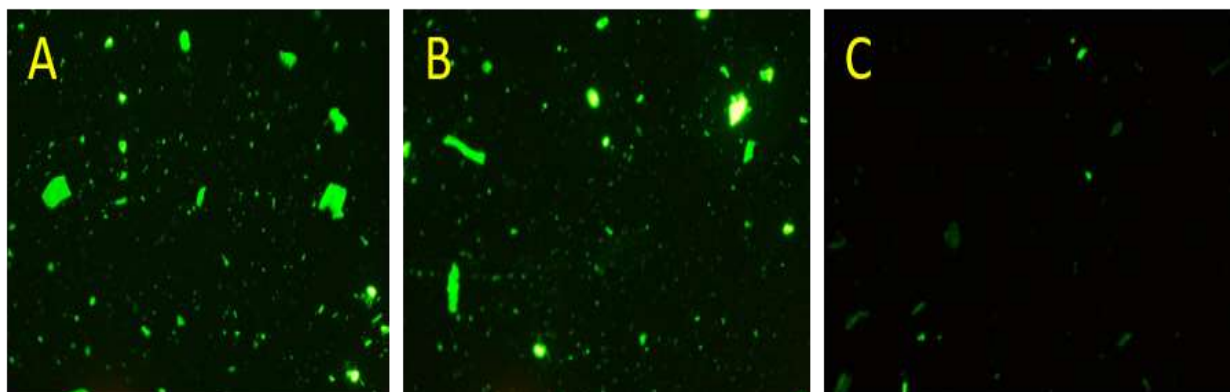


Figure 6.2 Images show fluorescence on gold surface of three different samples. Image A shows surface has APTES as linkers, fluorescent IgG solution (50ng/ml) stays on surface for 24 hours then flush surface. Image B has APTES as linkers, fluorescent IgG solution (5ng/ml) stays on surface for 24 hours then flush surface. Image 3 shows surface has no linkers; fluorescent IgG solution (50ng/ml) stays on surface for 24 hours.

All images from figure 6.1 and figure 6.2 are taken under microscope (10X) in fluorescence field with identical photographic settings. Based on this fact, we use Photoshop software to analyze the green fluorescence of each image. Photoshop can convert the intensity of green to numbers for each image from figure 6.1 and figure 6.2. Then, we extract all values and make a 3*2 table. From

table 1, we can see that the gold surface has APTES as linkers can bind more protein molecules. Therefore, the APTES method performs better on thermal-plasmonic substrate.

Table 6.1 Table contains 6 values of green color intensity which extracted from fluorescent microscope images. Each image can show the amount of fluorescent antibody B bind on surface of substrate.

	Value of Color Intensity in Green Histogram Channel		
	DSP	APTES	No Linker
50 ng/ml	19.54	26.67	3.47
5 ng/ml	14.25	25.81	2.46

After coated gold surface with linkers, we can anchor molecular probes on surface. Bovine IgG as molecular probes are immobilized on gold surface directly at first. However, the specific bindings between fluorophore conjugated anti-bovine IgG in sample and bovine IgG which has been immobilized on gold is going poorly (Figure 6.1). After study different methods that showing antibody immobilization on solid surface, we improve the method we use and introduce an extra protein molecule to bridge the linkers and the molecular probes. Normally, once an antibody molecule immobilizes on solid surface, it can partially lose its specific binding competence [62]. This phenomenon is due to random orientation of molecule on surface. Via using the Protein A as facilitator, it becomes possible to immobilize antibody in a fixed orientation (Figure 6.2). Once molecular probes can have orientated immobilization, resulting in much less hindrance for the binding site which for binding the fluorescent molecules.

By far, the molecular probes are orientated immobilized on substrate, allowing specific bindings to happen. Next, we introduce Opto-Fluidics in sample when it is incubated on substrate. To have better control over Opto-Fluidics and create a consistent environment for different samples, we

use the Opto-Fluidic chip which has PDMS mold with multiple wells structure (Figure 6.5). It is the same chip which is used in biocompatibility tests (Figure 4.1). Same volume of samples will be added into each well and use cover slip to fully cover the well during the incubation.

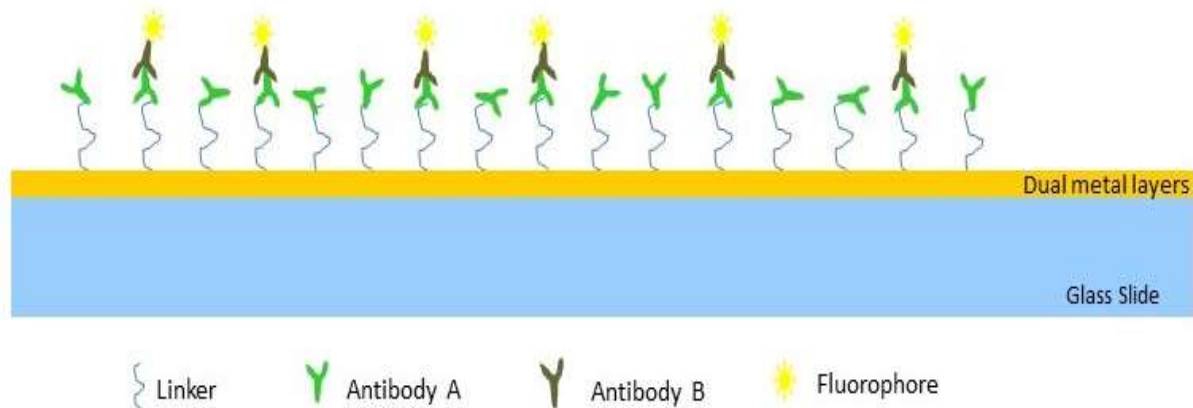


Figure 6.3 2-D sketch shows original molecule layer structure on plasmonic substrate. Fluorophore is conjugated with Antibody B (anti-bovine IgG). Antibody A (bovine IgG) directly binds to linkers with different orientation. Only a few Antibody B can find the binding site on antibody A and form specific binding.

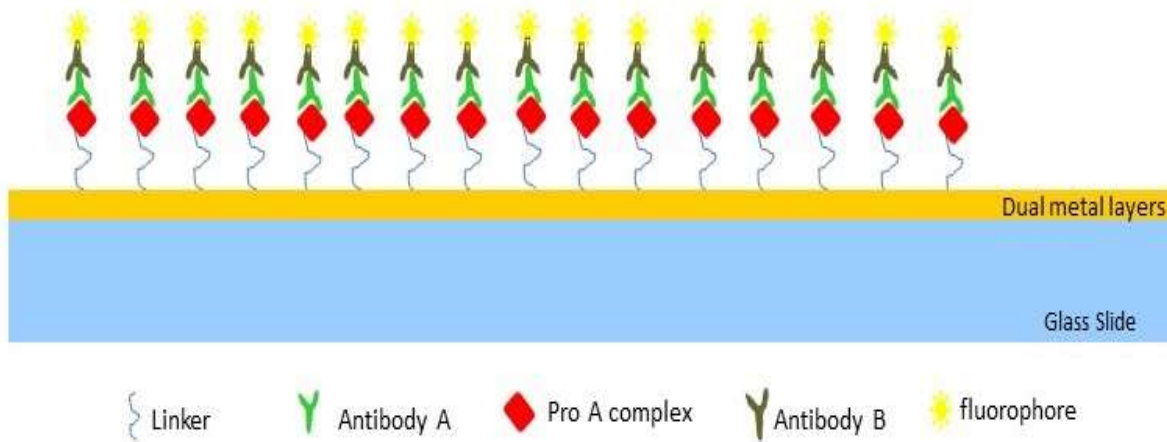


Figure 6.4 2-D sketch shows upgraded molecule layer structure on substrate. Antibody A bind to protein A in a fixed orientation. Binding sites on antibody A are free to bind with antibody B.

To identify whether Opto-Fluidics can act as micro-agitation and facilitate the specific bindings on surface, we set two groups of samples as a control test. Samples in group one has no Opto-Fluidics during incubation. Samples in group two has Opto-Fluidics during incubation. The

concentration of fluorescent protein in sample is 5 ng/ml. Laser power applied on each sample in experimental group is set as 20 mW.

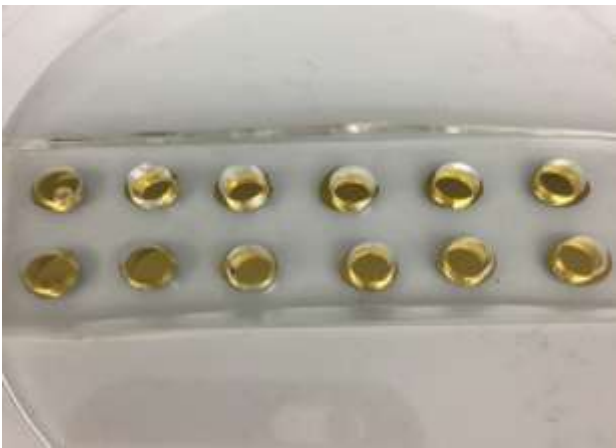


Figure 6.5 Image shows the Opto-Fluidic chip which is used in experiments. Each well has 40 ul capacity.

Again, we use Photoshop to accurately analyze the intensity of green fluorescence of each image. Values that represent the intensity of green for each image are extracted and composed into a line chart. This line chart can clearly demonstrate that the Opto-Fluidics can significantly facilitate the protein molecules specific bindings on surface within 30 minutes.

Table 6.2 Table contains 2*8 fluorescent microscope images. Each image can show the fluorescent attachments on the surface of substrate. Magnification is 10X. All images have the same photographic settings



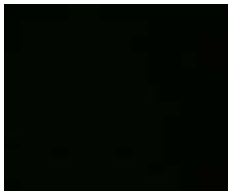









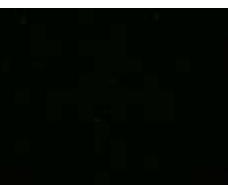

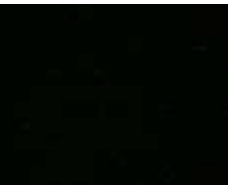

Time of Incubation	Incubation without Opto-Fluidics	Incubation with Opto-Fluidics
0 min		

Table 6.2 (Continued)

Time of Incubation	Incubation without Opto-Fluidics	Incubation with Opto-Fluidics
2 mins		
5 mins		
10 mins		
15 mins		
20 mins		
25 mins		
30 mins		

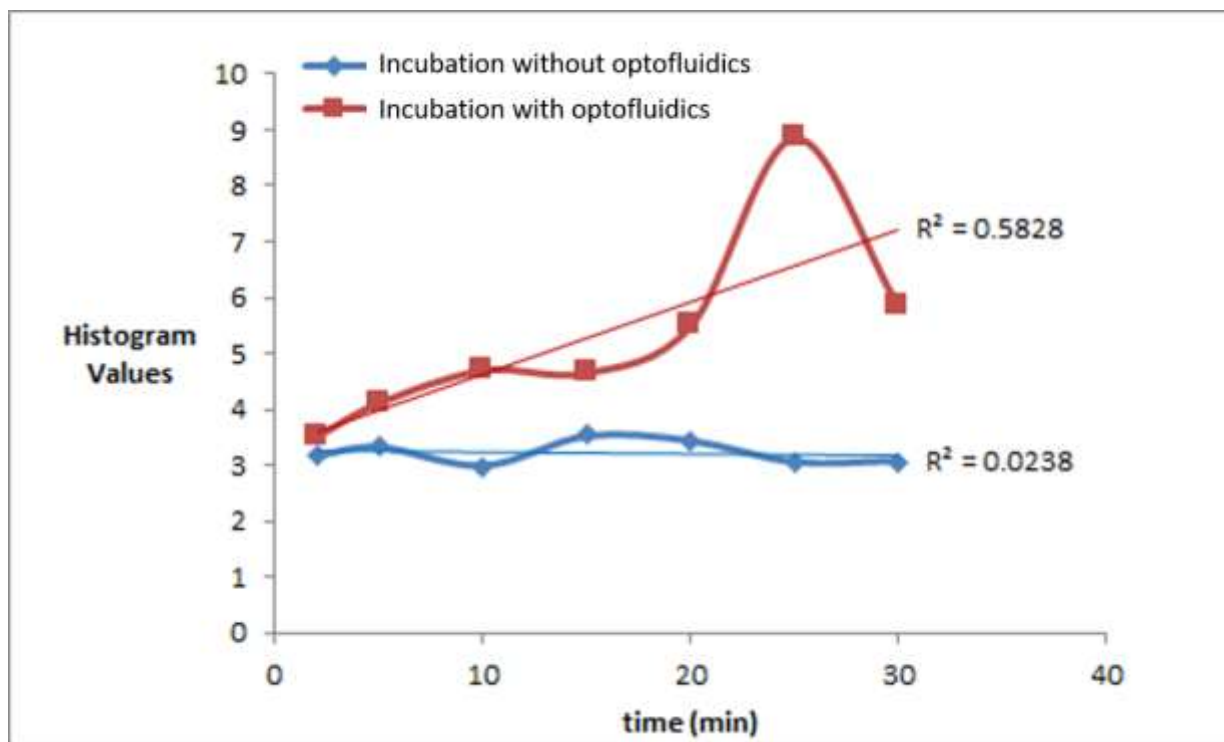


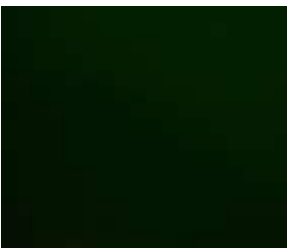
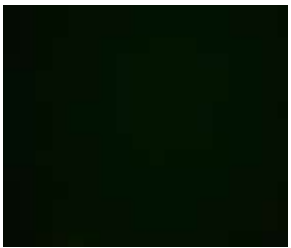







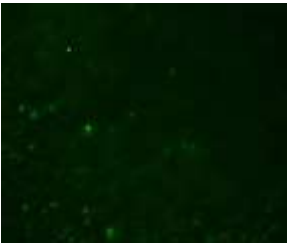


Figure 6.6 Line chart demonstrates Opto-Fluidics in sample can speed up fluorescent antibody attachment. This line chart contains two curves and 16 values. Blue curve shows background level of signal, which means there is very few hybridizations takes place in 30 minutes under normal condition. Red curve shows a rapid growth of fluorescence, which means molecules hybridizations are accelerated in the presence of Opto-Fluidics.

After we prove that Opto-Fluidics can facilitate specific bindings of protein molecules on solid surface. The following study is to identify the optimal power intensity of laser and the optimal length of time for treating sample by Opto-Fluidics. Fortunately, these are the only two variables in experiments. We set the longest time of treatment is 30 minutes. Different samples will be treated with different length with an interval setting of five minutes. There is no evidence can show that the longer time of treatment can lead to a better result. Because the bindings between multiple protein layers on gold are maintained by weak bonds (hydrogen bonds, hydrophobic force, etc). These bonds are easy to be broken with external forces. The Fluorescent protein which was captured before, might break away from probe and return free now and then, under the excessive micro-mixing fluids. So, we set three groups in this control experiment. Each group has different

length of time for sample incubation. Each group has four samples, and different sample is treated with different power intensity of laser. The concentration of fluorescent protein in sample is 50 ng/ml.

Table 6.3 Table contains 3*4 fluorescent microscope images. Each image can show the fluorescent light from surface of substrate. Magnification is 10X. All images have the same photographic settings.

	10 mins	20 mins	30 mins
20 mW			
50 mW			
80 mW			
110 mW			

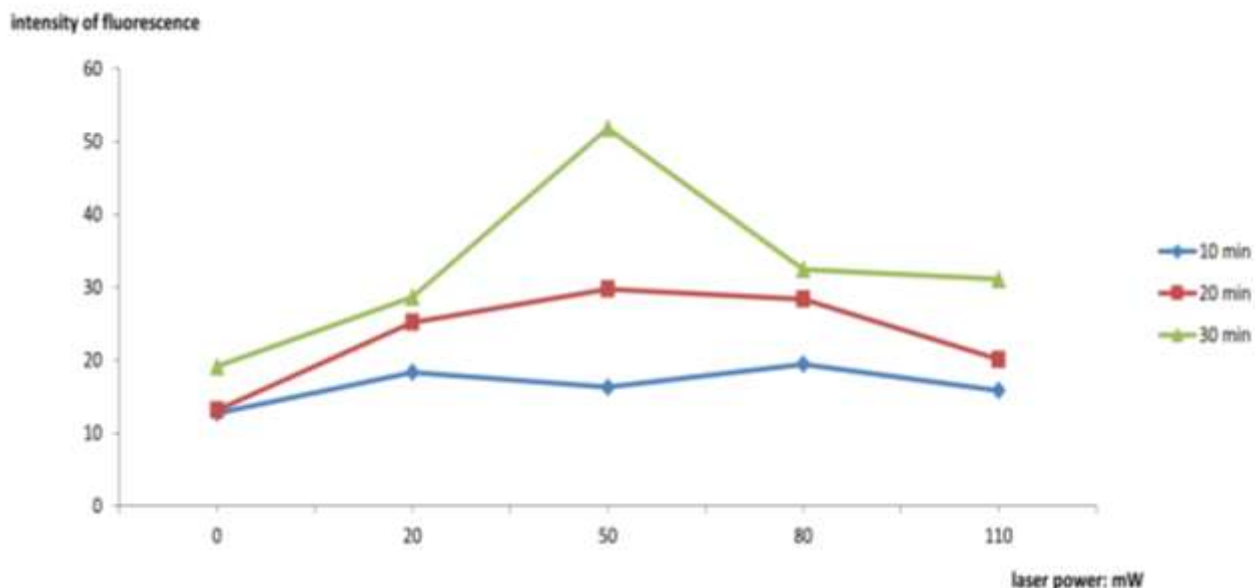


Figure 6.7 Line chart reveals the optimal settings of Opto-Fluidic treatment for the best outcome.

Line chart shows that it consists of 3 curves and 12 values. Blue curve shows a 10 minutes incubation with Opto-Fluidics with four different power do not show a noticeable change. Red line shows 20 minutes incubation incurs improvement on hybridization. But excessive power starts from 80 mW can inhibit hybridization. Green curve shows 30 minutes incubation cause significant improvement on hybridization. Meanwhile, hybridization on surface is impeded when laser power over 50 mW.

Based on the line chart above, we can conclude two results. First, the specific bindings of protein molecules on solid surface can be accelerated by using Opto-Fluidics. The prolonged treatment can incur a better result. But we only know that the 30 minutes as maximum length of treatment can perform best in experiment. Second, by given a fixed length of time of treatment, laser power set at medium level can incur the optimal result. Specifically, the optimal effect brought by Opto-Fluidics requires 50 mW laser power setting and 30 minutes of treatment. Compare with the sample that incubated for 30 minutes without Opto-Fluidics, the sample is treated by Opto-Fluidics with 50 mW power setting has an increased efficiency of specific bindings on surface by 2.5-fold at least.

Chapter 7: Accomplishments and Involvements in Other Projects

⁴7.1 Subcellular and in-vivo Nano-Endoscopy

In this project, a nanoendoscope is fabricated by applying wet-etching approach. The chemical composition of nanoendoscope is silica, that enable it to collect optical signals from individual cell or even organelle. Local fluorescence signals can be captured by this endoscope and propagates through optical wire and reaches to signal detector. I participate a serial of experiments that use nanoendoscope to detect fluorescence signal from single cells. We use green fluorescence dye to stain live cells. Then live cells can emit fluorescent signals. Next, we fix the nanoendoscope onto a delicate micro-manipulator to manipulate the movement of nanoendoscope. Use the manipulator to precisely move the endoscope and let the tip of it insert into a fluorescent cell. In this way, the fluorescence signal given by the cell can be absorbed into the nanoendoscope. Then signals can be conducted through optical fiber and be detected by a highly sensitive optical sensor (ultra-sensitive spectrometer). This groundbreaking work push the limit of optical signal detection of bio-samples down to the cellular level.

⁴This section was published in Scientific Reports...(Cheemalapati, Surya Venkatesekhar, et al. "Subcellular and in-vivo Nano-Endoscopy." Scientific reports 6 (2016): 34400.). Permission is included in Appendix: Copyright Permissions

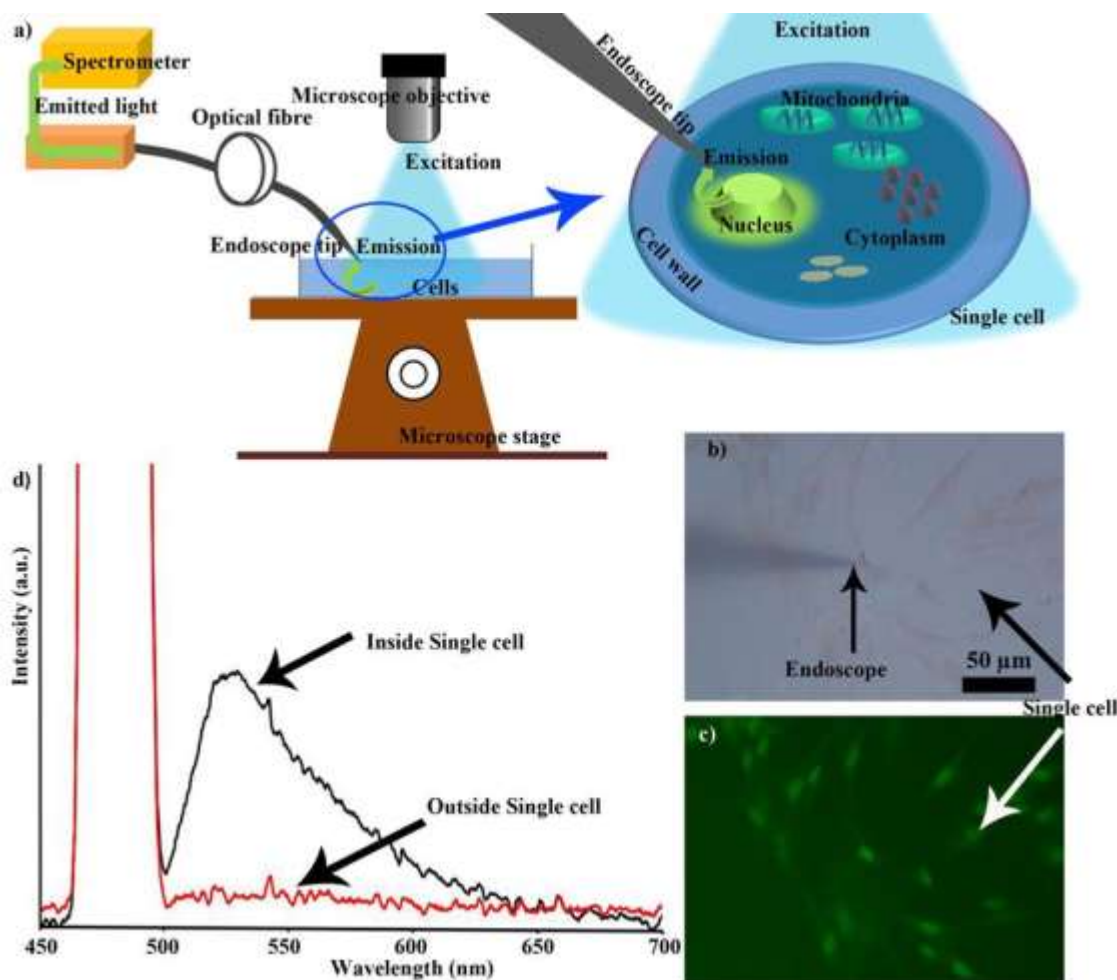


Figure 7.1 In vitro spectrum collection using nanoendoscope. a) Schematic of the experiment where internal microscope light source was used for fluorescence excitation. b) A bright field image showing the tip of nanoendoscope inserted into a fibroblast cell and c) the corresponding fluorescence image. d) The black curve is the spectrum (peak ~ 525 nm) collected from a single cell using nanoendoscope, while the red curve is the spectrum taken outside the cell. The Y axis shows intensity of green signal.

57.2 Plasmono-Magnetic Material for Precise Photothermal Heating

In this project, one type of magnetic microbeads which surface is coated with metal nanocages is designed and fabricated in lab. This type of magnetic microbeads can move under the influence of magnetic field. By control the direction of magnetic field, the movement of microparticles can

⁵This section was published in Royal Society of Chemistry...(Ladanov, Mikhail, et al. "Plasmono-magnetic material for precise photothermal heating." RSC advances 8.5 (2018): 2660-2666.). Permission is included in Appendix: Copyright Permissions

be controllable accordingly. Meanwhile, the magnetic microbeads can generate heat as long as they are under the exposure of NIR laser. This is because the surface magnetic microbead is coated with nanocages. When the NIR laser strikes on the surface of microbead, the nanocages can generate heat due to the thermo-plasmonic effect. By using the near infrared laser, magnetic microbeads, and controllable magnetic field, we design a serial of experiments that can implement precise destruction of single cell in vitro. In the experiment, we add the microbeads into the cell medium in petri-dish. Then we apply the controllable magnetic field around cell medium to guide microparticles move towards the target cell and form a microparticle aggregation around the target cell. Meanwhile, cells are attached to the surface of petri-dish and unable to move. Then we shine the NIR laser on the target cell, which is surrounded by the magnetic microbeads. Eventually, the local heat generated by the microbeads can induce the necrocytosis of target cell. These works demonstrate the feasibility of using magnetic microparticles to accurately kill targeted cells.

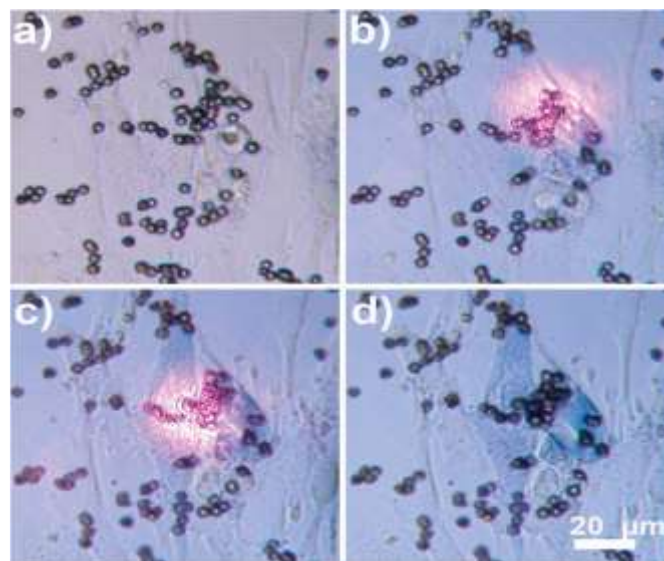


Figure 7.2 The necrocytosis of fibroblast cells induced by local heat. NIR light shines at a cluster of the nanocage-covered magnetic beads resting on top of a cell (~ 15 μm beads). a) Time - 0 min no light. b) after 10 min of continuous light irradiation, one cell is dead, and it is indicated by trypan blue dye from environment. c) After 20 min irradiation, more dye diffuses into the cell. Adjacent cell on left side also dead. d) laser turned off, two dead cells are in color blue show death meanwhile cells around free of irradiation are alive.

⁶7.3 Modular Microfluidic Filters Based on Transparent Membranes

In this project, a new type of microfluidic filter is designed and fabricated in our lab. The filter is made of silicon nitride and has a porous structure. This filter can make a fine separation of organic particles from liquid sample under low pressure. As a result, apply low pressure on filter can protect the integrity of filtered particles from rupture or any membrane damage. Since the membrane can filter cells out from bio samples, we need to test if the material and the structure of membrane will give any physical or chemical harms to cells. Therefore, we conduct a serial of experiments to test the biocompatibility of the filter membrane. First, the fibroblast cells suspension is prepared. Then let the cell suspension go through the filter, and the membrane can filter out fibroblast cells from sample. Next, leave the cells on membrane and nourish them by soaking the membrane in culture medium. As a result, we can see that cells which went through filtering process and stuck on membrane, are alive and attached to the membrane after 24 hours incubation. This work demonstrates the innovative filter membrane used for filtering bio samples has a good biocompatibility.

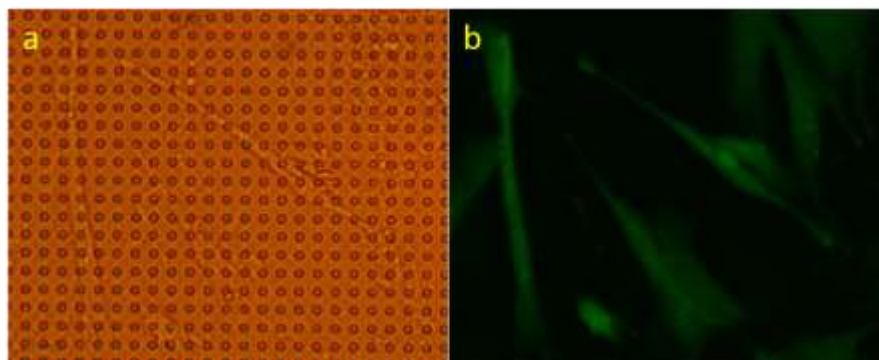


Figure 7.3 Human lung fibroblast cells captured and then grown for 3 days on the surface of microfilter membrane. a) Optical microscopy image of the membrane with cells. b) Fluorescence microscopy image of the cells demonstrate that all cells are alive with normal cellular morphology.

⁶This section was published in Journal of Electronic Packaging...(Archibong, E., et al. "Modular microfluidic filters based on transparent membranes." Journal of Electronic Packaging 138.4 (2016).). Permission is included in Appendix: Copyright Permissions

⁷7.4 Measurement of Thickness of Highly Inhomogeneous Crude Oil Slicks

In this project, we build up a set-up that can detect the thickness of oil slicks on water. This technology can be used to study the toxic effect of crude oil slicks on aquatic organisms. Based on the Beer-Lambert's law, we can measure the amount of laser attenuation after transmitting through oil layer, to estimate the local thickness of crude oil slick on top of saline water.

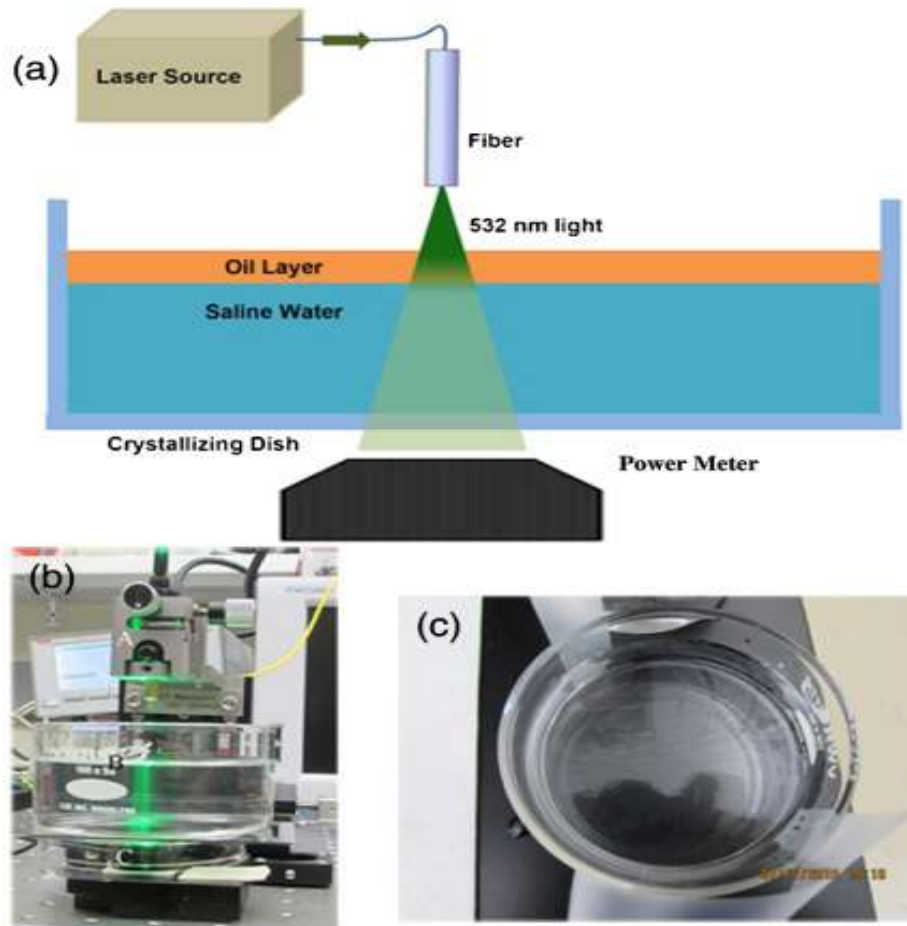


Figure 7.4 Measurement of the thickness of a slick generated on artificial seawater. (a) Schematic of the experimental setup. (b) Photograph of the experimental setup. Laser light is shining from an optical fiber and travels through an oil layer floating on the water surface in a crystallizing dish. Power is measured using a power meter placed under the crystallizing dish. (c) An image of a typical slick generated on the surface of artificial seawater.

⁷This section was published in Applied Optics...(Cheemalapati, Surya, et al. "Measurement of thickness of highly inhomogeneous crude oil slicks." Applied Optics 56.11 (2017): E72-E76.). Permission is included in Appendix: Copyright Permissions

References

- [1] Tkachenko, Georgiy, and Etienne Brasselet. "Optofluidic sorting of material chirality by chiral light." *Nature communications* 5.1 (2014): 1-7.
- [2] Paulsen, Kevin S., Dino Di Carlo, and Aram J. Chung. "Optofluidic fabrication for 3D-shaped particles." *Nature communications* 6.1 (2015): 1-9.
- [3] Archibong, Edikan, et al. "Design of an optofluidic sensor for rapid detection of hemolysis." *Sensors and Actuators B: Chemical* 288 (2019): 274-278.
- [4] Archibong, Edikan, Justin Stewart, and Anna Pyayt. "Optofluidic spectroscopy integrated on optical fiber platform." *Sensing and Bio-Sensing Research* 3 (2015): 1-6.
- [5] Esseling, Michael, et al. "Optofluidic droplet router." *Laser & Photonics Reviews* 9.1(2015): 98-104.
- [6] Kim, Minkyu, et al. "Optofluidic ultrahigh-throughput detection of fluorescent drops." *Lab on a Chip* 15.6 (2015): 1417-1423.
- [7] Mishra, Kartikeya, Dirk Van den Ende, and Frieder Mugele. "Recent developments in optofluidic lens technology." *Micromachines* 7.6 (2016): 102.
- [8] Zhu, Xiangchao, et al. "Optofluidic chromatography: label-free sorting of exosomes with plasmonic microlenses." *Optical Trapping and Optical Micromanipulation XVI*. Vol. 11083. International Society for Optics and Photonics, 2019.
- [9] Coskun, Ahmet F., et al. "Lensfree optofluidic plasmonic sensor for real-time and label-free monitoring of molecular binding events over a wide field-of-view." *Scientific reports* 4 (2014): 6789.
- [10] Ko, Jina, et al. "Smartphone-enabled optofluidic exosome diagnostic for concussion recovery." *Scientific reports* 6 (2016): 31215.
- [11] Roxworthy, Brian J., et al. "Understanding and controlling plasmon-induced convection." *Nature communications* 5.1 (2014): 1-8.
- [12] Palermo, Giovanna, et al. "Flexible thermo-plasmonics: An opto-mechanical control of the heat generated at the nanoscale." *Nanoscale* 10.35 (2018): 16556-16561.

- [13] Miao, X.; Wilson, B.K.; Lin, L.Y. Localized surface plasmon assisted microfluidic mixing. *Appl. Phys. Lett.* 2008, 92, 124108.
- [14] Donner, J.S.; Baffou, G.; McCloskey, D.; Quidant, R. Plasmon-assisted optofluidics. *ACS Nano* 2011, 5, 5457–5462.
- [15] Chen, J.; Kang, Z.; Kong, S.K.; Ho, H.P. Plasmonic random nanostructures on fiber tip for trapping live cells and colloidal particles. *Opt. Lett.* 2015, 40, 3926–3929.
- [16] Kang, Z.; Chen, J.; Wu, S.Y.; Chen, K.; Kong, S.K.; Yong, K.T.; Ho, H.P. Trapping and assembling of particles and live cells on large-scale random gold nano-island substrates. *Sci. Rep.* 2015, 5, 9978.
- [17] Lozan, O.; Perrin, M.; Ea-Kim, B.; Rampnoux, J.M.; Dilhaire, S.; Lalanne, P. Anomalous light absorption around subwavelength apertures in metal films. *Phys. Rev. Lett.* 2014, 112, 193903.
- [18] Meier, M.; Wokaun, A.; Liao, P.F. Enhanced fields on rough surfaces: dipolar interactions among particles of sizes exceeding the Rayleigh limit. *JOSA B* 1985, 2, 931–949.
- [19] Norman, T.J.; Grant, C.D.; Magana, D.; Zhang, J.Z.; Liu, J.; Cao, D.; Bridges, F.; Van Buuren, A. Near infrared optical absorption of gold nanoparticle aggregates. *J. Phys. Chem. B* 2002, 106, 7005–7012.
- [20] Winkas, John T., et al. "Different Regimes of Opto-fluidics for Biological Manipulation." *Micromachines* 10.12 (2019): 802.
- [21] Hao Wang., et al. "Innovative optofluidics and microscopy-based rapid analysis of pathogens," *Biomed. Opt. Express* 11, 5060-5069 (2020)
- [22] Lee, W.R.; Oh, K.T.; Park, S.Y.; Yoo, N.Y.; Ahn, Y.S.; Lee, D.H.; Youn, Y.S.; Lee, D.K.; Cha, K.H.; Lee, E.S. Magnetic levitating polymeric nano/microparticulate substrates for three-dimensional tumor cell culture. *Colloids Surf. B Biointerf.* 2011, 85, 379–384.
- [23] Durmus, N.G.; Tekin, H.C.; Guven, S.; Sridhar, K.; Yildiz, A.A.; Calibasi, G.; Ghiran, I.; Davis, R.W.; Steinmetz, L.M.; Demirci, U. Magnetic levitation of single cells. *Proc. Natl. Acad. Sci. USA* 2015, 112, E3661–E3668.
- [24] Thoumine, O.; Ott, A.; Cardoso, O.; Meister, J.J. Microplates: a new tool for manipulation and mechanical perturbation of individual cells. *J. Biochem. Biophys. Methods* 1999, 39, 47–62.
- [25] Korda, P.T.; Taylor, M.B.; Grier, D.G. Kinetically locked-in colloidal transport in an array of optical tweezers. *Phys. Rev. Lett.* 2002, 89, 128301.
- [26] Schuller, J.A.; Barnard, E.S.; Cai, W.; Jun, Y.C.; White, J.S.; Brongersma, M.L. Plasmonics for extreme light concentration and manipulation. *Nat. Mater.* 2010, 9, 193.

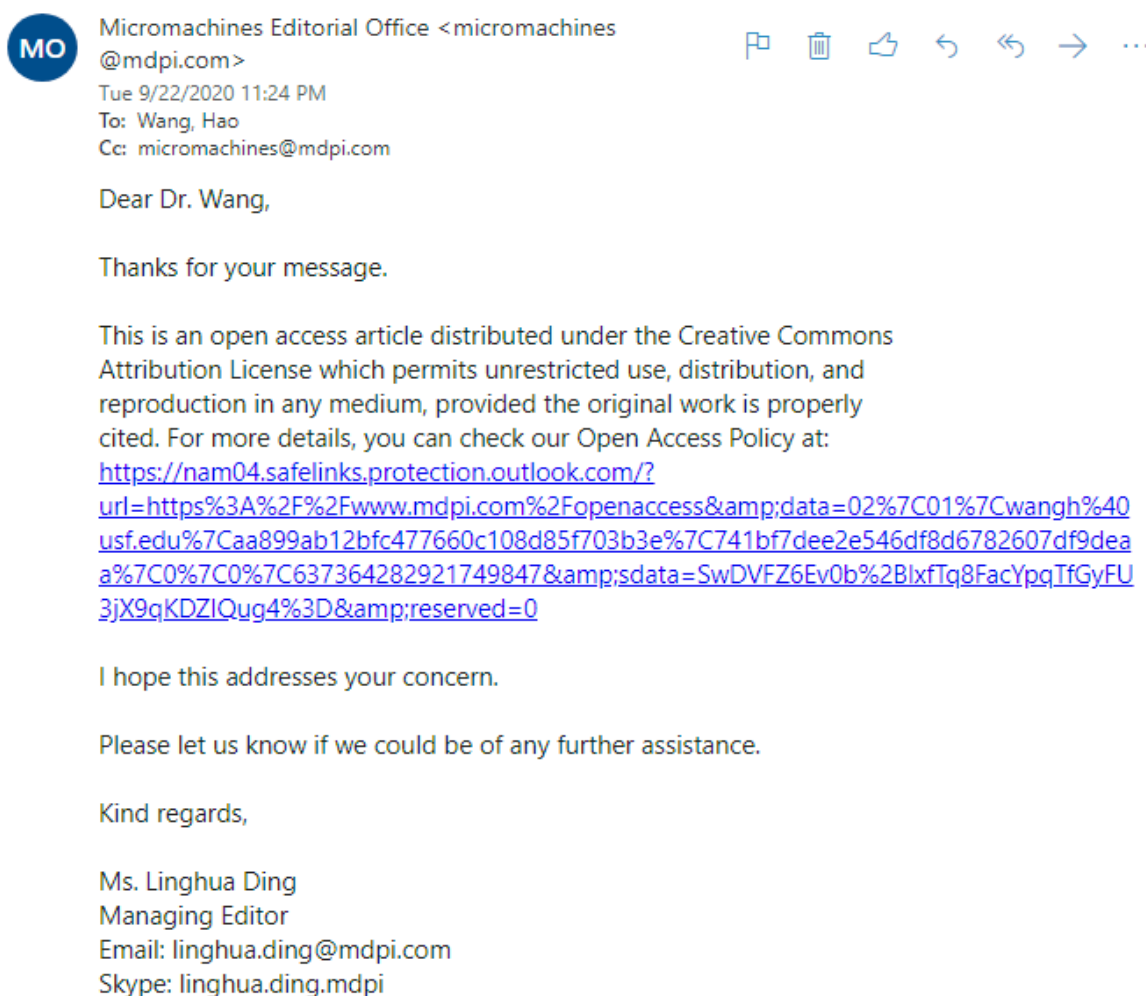
- [27] Kurup, G.K.; Basu, A.S. Rolling, aligning, and trapping droplets on a laser beam using marangoni optofluidic tweezers. In Proceedings of the 16th International Conference Solid-State Sensors, Actuators and Microsystems (TRANSDUCERS), Beijing, China, 5–9 June 2011; pp. 266–269.
- [28] Khan, I.; Tang, E.; Arany, P. Molecular pathway of near-infrared laser phototoxicity involves ATF-4 orchestrated ER stress. *Sci. Rep.* 2015, 5, 10581.
- [29] Berthelot, J.; Aćimović, S.S.; Juan, M.L.; Kreuzer, M.P.; Renger, J.; Quidant, R. Three-dimensional manipulation with scanning near-field optical nanotweezers. *Nat. Nanotechnol.* 2014, 9, 295–299.
- [30] Mandal, S.; Serey, X.; Erickson, D. Nanomanipulation using silicon photonic crystal resonators. *Nano Lett.* 2009, 10, 99–104.
- [31] Liu, Y.; Cheng, D.K.; Sonek, G.J.; Berns, M.W.; Chapman, C.F.; Tromberg, B.J. Evidence for localized cell heating induced by infrared optical tweezers. *Biophys. J.* 1995, 68, 2137–2144.
- [32] Khan, I.; Tang, E.; Arany, P. Molecular pathway of near-infrared laser phototoxicity involves ATF-4 orchestrated ER stress. *Sci. Rep.* 2015, 5, 1058
- [33] Chiou, P.Y.; Ohta, A.T.; Wu, M.C. Massively parallel manipulation of single cells and microparticles using optical images. *Nature* 2005, 436, 370.
- [34] Kurup, G.K.; Basu, A.S. Hydrodynamic particle concentration inside a microfluidic plug. In Proceedings of the 14th International Conference on Miniaturized Systems for Chemistry and Life Sciences (MicroTAS), Groningen, The Netherlands, 3–7 October 2010; pp. 740–742.
- [35] Trivedi, V.; Doshi, A.; Kurup, G.K.; Ereifej, E.; Vandevord, P.J.; Basu, A.S. A modular approach for the generation, storage, mixing, and detection of droplet libraries for high throughput screening. *Lab Chip* 2010, 10, 2433–2442.
- [36] Jeong, Y.G.; Lee, J.S.; Shim, J.K.; Hur, W. A scaffold-free surface culture of B16F10 murine melanoma cells based on magnetic levitation. *Cytotechnology* 2016, 68, 2323–2334.
- [37] Namura, K.; Imafuku, S.; Kumar, S.; Nakajima, K.; Sakakura, M.; Suzuki, M. Direction control of quasi-stokeslet induced by thermoplasmonic heating of a water vapor microbubble. *Sci. Rep.* 2019, 9, 4770.
- [38] Flores-Flores, E.; Torres-Hurtado, S.A.; Páez, R.; Ruiz, U.; Beltrán-Pérez, G.; Neale, S.L.; Ramirez-San-Juan, J.C.; Ramos-García, R. Trapping and manipulation of microparticles using laser-induced convection currents and photophoresis. *Biomed. Opt. Express* 2015, 6, 4079–4087.39.

- [39] Kumar, Rajagopal, and Fenil Chetankumar Panwala. "Micropatterning in BioMEMS for Separation of Cells/Bioparticles." *MEMS Sensors: Design and Application* (2018): 71.
- [40] Ekstrom, Bjorn, et al. "Microfluidic structure and process for its manufacture." U.S. Patent No. 5,376,252. 27 Dec. 1994.
- [41] Shields CW 4th, Ohiri KA, Szott LM, López GP. Translating microfluidics: Cell separation technologies and their barriers to commercialization. *Cytometry B Clin Cytom.* 2017;92(2):115-125. doi:10.1002/cyto.b.21388
- [42] E. K. Stevenson, A. R. Rubenstein, G. T. Radin, R. S. Wiener, and A. J. Walkey, "Two decades of mortality trends among patients with severe sepsis: a comparative meta-analysis," *Crit. Care Med.* 42(3), 625–631 (2014)
- [43] G. Kumar, N. Kumar, A. Taneja, T. Kaleekal, S. Tarima, E. McGinley, E. Jimenez, A. Mohan, R. A. Khan, J. Whittle, and E. Jacobs, "Nationwide trends of severe sepsis in the 21st century (2000–2007)," *Chest* 140(5), 1223–1231 (2011)
- [44] Gizem Polat and Rustem Anil Ugan, "Sepsis and Septic Shock: Current Treatment Strategies and New Approaches," *Eurasian J. Med.* 49, 53–58 2017.
- [45] S. Y. Liang and A Kumar,, "Empiric antimicrobial therapy in severe sepsis and septic shock: optimizing pathogen clearance," *Curr. Infect. Dis. Rep.*, 17(7), 36 (2015).
- [46] I. M. Sheldon, "Detection of Pathogens in Blood for Diagnosis of Sepsis and Beyond," *EBioMedicine* 9, 13–14 (2016).
- [47] L. B. Reller, M. Weinstein, J. H. Jorgensen, and M. J. Ferraro, "Antimicrobial susceptibility testing: a review of general principles and contemporary practices," *Clin. Infect. Dis.* 49(11), 1749–1755 (2009).
- [48] L. E. Lehmann, K. P. Hunfeld, T. Emrich, G. Haberhausen, H. Wissing, A. Hoeft, and F. Stüber, "A multiplex real-time PCR assay for rapid detection and differentiation of 25 bacterial and fungal pathogens from whole blood samples," *Med. Microbiol. Immunol.* 197(3), 313–324 (2008).
- [49] Suberviola, A. Marquez-Lopez, A. Castellanos-Ortega, C. Fernandez-Mazarrasa, M. Santibanez, and L. M.Martinez, "Microbiological Diagnosis of Sepsis: Polymerase Chain Reaction System Versus Blood Cultures," *Am J Crit Care.* 25(1), 68–75 (2016).
- [50] P. A. Demirev, Y. P. Ho, V. Ryzhov, and C. Fenselau, "Microorganism identification by mass spectrometry and protein database searches," *Anal. Chem.* 71(14), 2732–2738 (1999).
- [51] Atul Kothari, Margie Morgan, and David Haake, "Emerging technologies for rapid identification of bloodstream pathogens," *Clinical Infectious Diseases* (2014): ciu292.

- [52] T. H. Huang, X. Ning, X. Wang, Murthy, Y. L. Tzeng, and R. M. Dickson, "Rapid cytometric antibiotic susceptibility testing utilizing adaptive multidimensional statistical metrics," *Anal. Chem.* 87(3), 1941–1949 (2015)
- [53] M. Cartwright, M. Rottman, N. I. Shapiro, B. Seiler, P. Lombardo, N. Gamini, J. Tomolonis, A. L. Watters, A. Waterhouse, D. Leslie, D. Bolgen, A. Graveline, J. H. Kang, T. Didar, N. Dimitrakakis, D. Cartwright, M. Super, and D. E. Ingber, "A Broad-Spectrum Infection Diagnostic that Detects Pathogen-Associated Molecular Patterns(PAMPs) in Whole Blood," *EBioMedicine.* 9, 217–227 (2016).
- [54] C. C. Neacsu, J. Dreyer, N. Behr, and M. B Raschke,, "Scanning-probe Raman spectroscopy with single-molecule sensitivity," *Phys. Rev. B* 73(19), 193406 (2006).
- [55] W. Ho, "Single-molecule chemistry," *J. Chem. Phys.* 117(24), 11033–11061 (2002).
- [56] T. Liu, Y. Lu, V. Gau, J. C. Liao, and P. K. Wong, "Rapid antimicrobial susceptibility testing with electrokinetics enhanced biosensors for diagnosis of acute bacterial infections," *Ann. Biomed. Eng.* 42(11), 2314–2321 (2014).
- [57] L. D'Amico, N. J. Ajami, J. A. Adachi, P. R. C. Gascoyne, and J. F. Petrosino, "Isolation and concentration of bacteria from blood using microfluidic membraneless dialysis and dielectrophoresis," *Lab Chip* 17(7), 1340–1348 (2017).
- [58] M. A. Faridi, H. Ramachandraiah, I. Banerjee, S. Ardabili, S. Zelenin, and A. Russom, "Elasto-inertial microfluidics for bacteria separation from whole blood for sepsis diagnostics," *J. Nanobiotechnol.* 15(1), 3 (2017).
- [59] Toegl, Andreas, et al. "Enhancing results of microarray hybridizations through microagitation." *Journal of biomolecular techniques: JBT* 14.3 (2003): 197.
- [60] Sankaranarayanan, Subramanian KRS, et al. "Flow induced by acoustic streaming on surface-acoustic-wave devices and its application in biofouling removal: A computational study and comparisons to experiment." *Physical Review E* 77.6 (2008): 066308.
- [61] Zhang, Yingying, et al. "Plasma membrane changes during programmed cell deaths." *Cell research* 28.1 (2018): 9-21.
- [62] Schmid, A. Hirlekar, et al. "Site-directed antibody immobilization on gold substrate for surface plasmon resonance sensors." *Sensors and Actuators B: Chemical* 113.1 (2006): 297-303.

Appendix 1: Copyright Permissions

The permission below is for the use of published content in Chapter 1



The permission below is for the use of published content in Chapter 2



pubscopyright <copyright@osa.org>

Mon 10/5/2020 11:32 AM

To: Wang, Hao; pubscopyright <copyright@osa.org>



Dear Hao Wang,

Thanks you for contacting The Optical Society.

OSA allows authors to include their papers in a theses with appropriate attribution. In this case, the attribution cannot yet name Applied Optics. If the thesis is still in progress then you may be able to update the citation after the manuscript receives a final decision from AO. Otherwise the manuscript should be cited as "in preparation".

Please let me know if you have any additional questions.

Kind Regards,
Hannah Greenwood

Hannah Greenwood
October 5, 2020
Authorized Agent, The Optical Society

The Optical Society (OSA)
[2010 Massachusetts Ave., NW](#)
[Washington, DC 20036 USA](#)
www.osa.org

Reflecting a Century of Innovation

...

The permission below is for the use of published content in Chapter 5



pubscopyright <copyright@osa.org>

Mon 8/24/2020 12:49 PM

To: Wang, Hao; pubscopyright <copyright@osa.org>



Dear Dr. Wang,

Thank you for your response.

For the use of material from Hao Wang, Priyanka Shiveshwarkar, Robert Brzozowski, Arseny Zhdanov, Shulin Shi, Prahathees Eswara, and Anna Pyayt, "Innovative optofluidics and microscopy-based rapid analysis of pathogens," Biomed. Opt. Express 11, 5060-5069 (2020)

Because you are the author of the source paper from which you wish to reproduce material, OSA considers your requested use of its copyrighted materials to be permissible within the author rights granted in the Copyright Transfer Agreement submitted by the requester on acceptance for publication of his/her manuscript. It is requested that a complete citation of the original material be included in any publication. This permission assumes that the material was not reproduced from another source when published in the original publication.

For the use of this paper in your thesis, it is permissible to use the version of record.

While your publisher should be able to provide additional guidance, OSA prefers the below citation formats:

For citations in figure captions:

[Reprinted/Adapted] with permission from [ref #] © The Optical Society. (Please include the full citation in your reference list)

For images without captions:

Journal Vol. #, first page (year published) An example: Opt. Express 19, 2720 (2011)

Please let me know if you have any questions.

Kind Regards,
Hannah Greenwood

Hannah Greenwood
August 24, 2020
Authorized Agent, The Optical Society

The Optical Society (OSA)
2010 Massachusetts Ave., NW
Washington, DC 20036 USA
www.osa.org

Reflecting a Century of Innovation

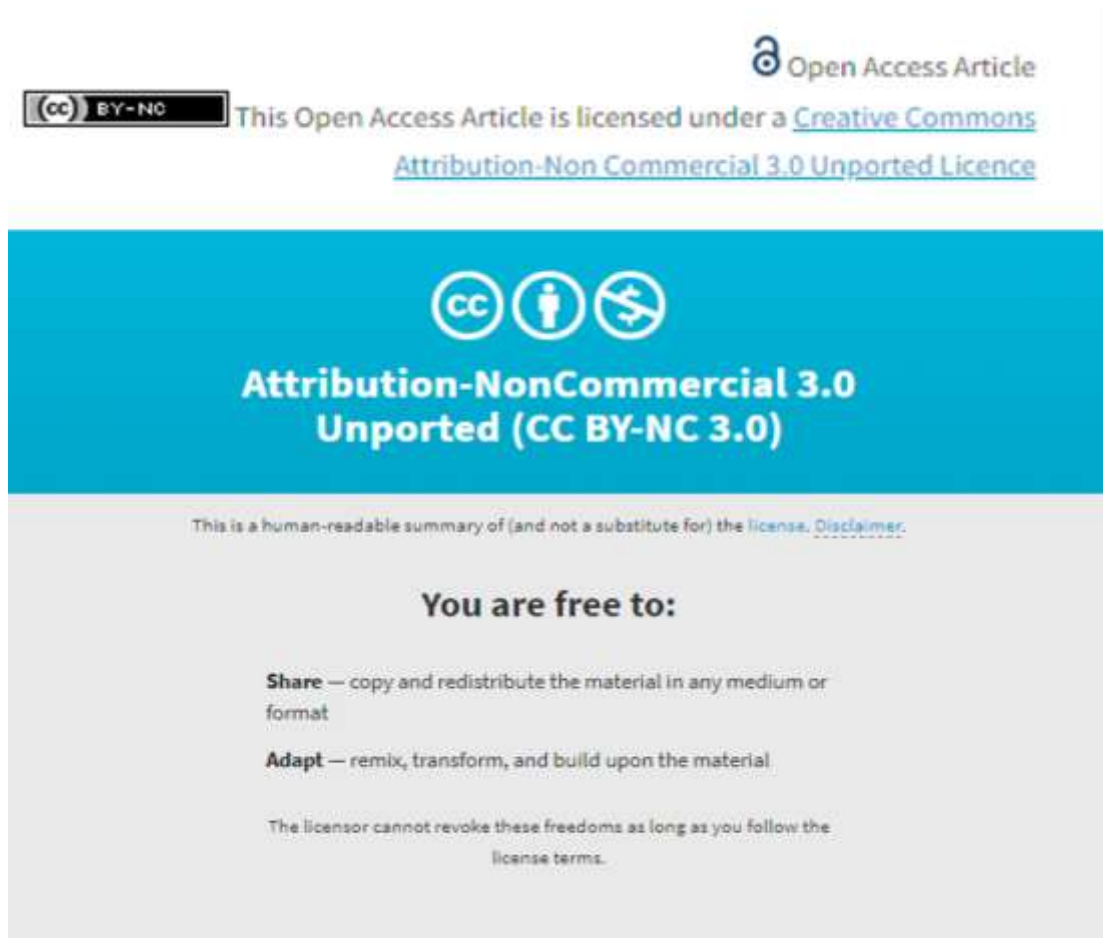
The permission below is for the use of Figure 7.1.

License agreement and author copyright

Scientific Reports does not require authors to assign copyright of their published original research papers to the journal. Articles are published under a [CC BY license](#) (Creative Commons Attribution 4.0 International License). The CC BY license allows for maximum dissemination and re-use of open access materials and is preferred by many research funding bodies. Under this license, users are free to share (copy, distribute and transmit) and remix (adapt) the contribution including for commercial purposes, providing they attribute the contribution in the manner specified by the author or licensor ([read full legal code](#)).

Visit our open research site for more information about [Creative Commons](#) licensing.

The permission below is for the use of Figure 7.2



The permission below is for the use of Figure 7.3



Beth Darchi <DarchiB@asme.org>

Tue 11/17/2020 2:12 PM

To: Wang, Hao



Dear Mr. Wang,

It is our pleasure to grant you permission to use the ASME **Figure 8** from “Modular Microfluidic Filters Based on Transparent Membranes,” by E. Archibong, H. Tuazon, H. Wang, J. Winkas, A. L. Pyayt, J. Electron. Packag. December 2016, 138(4), cited in your letter for inclusion in a doctoral dissertation to be published by University of South Florida.

Permission is granted for the specific use as stated herein and does not permit further use of the materials without proper authorization. Proper attribution must be made to the author(s) of the materials. **Please note:** if any or all of the figures and/or Tables are of another source, permission should be granted from that outside source or include the reference of the original source. ASME does not grant permission for outside source material that may be referenced in the ASME works.

As is customary, we request that you ensure full acknowledgment of this material, the author(s), source and ASME as original publisher.

Many thanks for your interest in ASME publications.

Sincerely,

Beth Darchi

Publishing Administrator

ASME

[2 Park Avenue](#)

[New York, NY 10016-5990](#)

The permission below is for the use of Figure 7.4

OSA Open Access License for OSA-Formatted Journal Article PDFs

An OSA-formatted open access journal article PDF may be governed by the [OSA Open Access Publishing Agreement](#) signed by the author and any applicable copyright laws. Authors and readers may use, reuse, and build upon the article, or use it for text or data mining without asking prior permission from the publisher or the Author(s), as long as the purpose is non-commercial and appropriate attribution is maintained.